Accepted manuscript:

Regional variations in fluid formation and metal sources in MVT mineralization in the Pennine Orefield, UK: Implications from rare earth element and yttrium distribution, Sr-Nd isotopes and fluid inclusion compositions of hydrothermal vein fluorites

by

Dennis Kraemer[*1], Sebastian Viehmann[2], David Banks[3], Anjani D. Sumoondur[1], Christian Koeberl[4, 5],Michael Bau[1]

1 Department of Physics and Earth Sciences, Jacobs University Bremen, Campus Ring 1, 28759 Bremen, Germany
2 Department of Geodynamics and Sedimentology, University of Vienna, Althanstraße 14, 1090 Vienna, Austria
3 University of Leeds, School of Earth and Environment, Woodhouse Lane, Leeds, UK
4 Department for Lithospheric Research, University of Vienna, Althanstraße 14, 1090 Vienna
5 Natural History Museum, Burgring 7, 1010 Vienna, Austria

https://doi.org/10.1016/j.oregeorev.2019.03.014

Received 29 October 2018; Received in revised form 26 February 2019; Accepted 11 March 2019 Available online 12 March 2019 (Embargo 24 months)

Regional variations in fluid formation and metal sources in MVT mineralization in the Pennine Orefield, UK: Implications from rare earth element and yttrium distribution, Sr-Nd isotopes and fluid inclusion compositions of hydrothermal vein fluorites

Dennis Kraemer*[1], Sebastian Viehmann[2], David Banks[3], Anjani D. Sumoondur[1], Christian Koeberl[4, 5], Michael Bau[1]

[1] Department of Physics and Earth Sciences, Jacobs University Bremen, Campus Ring 1, 28759 Bremen, Germany

[2] Department of Geodynamics and Sedimentology, University of Vienna, Althanstraße 14, 1090 Vienna, Austria

[3] University of Leeds, School of Earth and Environment, Woodhouse Lane, Leeds, UK

[4] Department for Lithospheric Research, University of Vienna, Althanstraße 14, 1090 Vienna

[5] Natural History Museum, Burgring 7, 1010 Vienna, Austria

* d.kraemer@jacobs-university.de; ORCID: https://orcid.org/0000-0001-8690-5211

Keywords: Pennine Orefield, Mississippi-Valley Type deposits, fluorite, rare earth elements, Eu geothermometry, Sr and Nd isotopes in IF- G and JDo-1

Abstract

The Pennine Orefield is one of the most important ore fields for Pb-Zn-Ba-F mineralization in Great Britain. It is subdivided into the Northern Pennine Orefield (NPO), consisting of the Alston and Askrigg Blocks, and the Southern Pennine Orefield (SPO). The Alston Block is underlain by the early Devonian Weardale Granite and the Askrigg Block by the coeval Wensleydale Granite. The potential

relationship between the batholiths and the mineralization is a matter of debate. We here studied the rare earth elements and Y (REY) geochemistry, Sr-Nd isotopes and fluid inclusion (FI) compositions of fluorites from the two structural blocks in the NPO and found that the fluorite mineralization in these blocks differ substantially. The REY in Askrigg fluorites show features that are characteristic for leaching of adjacent Lower Carboniferous limestones. In contrast, Alston fluorites have significantly higher REY concentrations, lack REY_{SN} limestone signatures and show a decoupling of redox-sensitive Eu from its trivalent REY 'neighbours'. Neodymium isotopes indicate a similar crustal source of REY in both blocks, but higher REY concentrations and lower Y/Ho ratios suggest Lower Carboniferous shales as potential REY source in the Alston Block. The fluids that precipitated the Alston fluorites experienced temperatures >250°C prior to mineral formation, as evidenced by Eu geothermometry. Fluorite *formation*, however, occurred at much lower temperatures, as suggested by homogenization temperatures in FI, that fall within ranges of 105-159°C in Alston and 99-160°C in Askrigg fluorites. Mineralization of the Mississippi-Valley Type usually lack association with igneous activity. We show that some of the fluids responsible for the NPO mineralization were influenced by magmatic sources. The REY systematics in Alston fluorites may be linked to an interaction of the Permian-age *Whin Sill* dolerite with the basement granite, which heated fluids and focussed fluid flow into the overlying sedimentary rocks. In the Askrigg Block, where such a dolerite intrusion was not described, fluorites lack any positive Eu_{SN} anomalies, indicating that these fluids had never been subjected to temperatures exceeding 200-250°C.

1. Introduction

The mineral fluorite (CaF_2) may serve as a valuable tool for deciphering the formation history of mineral deposits. Fluorite minerals preserve, for example, the rare earth element and yttrium (REY) patterns and Sr-Nd isotope fingerprint of a hydrothermal fluid from which they precipitated and, hence, can be used as reliable geochemical archives to reconstruct the physicochemical parameters of ancient and modern hydrothermal systems (Bau and Dulski, 1995; Göb et al., 2013; Loges et al.,

2012; Schwinn and Markl, 2005). The REY are strongly complexed with fluoride in F-rich hydrothermal fluids, which may lead to a significant enrichment of REY in F-bearing hydrothermal fluids and in fluorite (Bau et al., 2003; Bilal and Langer, 1987) due to numerous substitution reactions (e.g., 2 Ca^{2+} ↔ REY^{3+} + Na^{+}; Bilal and Langer 1987; Möller 1998; Bau et al. 2003). However, complexation of REY in F-rich fluids is strongly dependent on the pH and temperature of the fluid (Williams-Jones et al., 2012). The analysis of REY in Ca-bearing minerals such as fluorite may therefore provide important information on metal sources, temperature conditions, fluid migration, host rock interaction and the chemical composition of the fluid phase (Bau et al., 2003; Castorina et al., 2008; Möller et al., 1982; Sánchez et al., 2010; Schwinn and Markl, 2005). Understanding ancient and modern hydrothermal systems and their specific chemistries, in turn, is essential for accurate and detailed models for ore deposit formation, which may facilitate the discovery of mineral deposits.

In this study, fluorites from the Alston and Askrigg blocks of the Northern Pennine Orefield (NPO) were investigated for their REY geochemistry, Sr and Nd isotopes and fluid inclusion compositions. The mineralization in the Pennine Orefield is considered a fluorine-bearing sub-type of Mississippi Valley Type (MVT) mineralization (Colman et al., 1989). Mississippi-Valley-Type mineralization usually forms through precipitation from mildly hot hydrothermal basinal brines (100-200°C) with relatively high fluid salinities (15-25wt.-% NaCl equivalent; Leach et al., 2001). These epigenetic ore deposits form predominantly in dolostone, but also in limestone and sandstone, and are globally important sources of lead and zinc sulphides; occasionally MVT deposits are significantly enriched in fluorite (Leach et al., 2001). MVT mineralization usually lacks a genetic affinity to igneous activity (Leach et al., 2001).

Fluorite-rich veins are widespread in the Variscan basement of Central and Western Europe. Important examples are found in the Massif Central (Munoz et al., 2005; Sizaret et al., 2004), in the Hercynian massifs of Spain (Galindo et al., 1994; Piqué et al., 2008; Sánchez et al., 2010; Tornos et al., 2000) and of Germany (Behr et al., 1987; Lüders and Möller, 1992; Schwinn and Markl, 2005).

Muchez et al. (2005) suggest that the major basin-hosted deposits in Europe are related to extensional tectonics and that the mineralizing fluids, which originated as (evaporated) seawater, intruded downward into the basin through interconnected fractures. The ore-bearing fluids were then expelled along extensional faults in regions characterized by pronounced extension and heat production (Muchez et al., 2005). Staude et al. (2009) suggested a model explaining intense fluid generation due to extensional tectonics. As a function of differences in compressibility between rocks and fluid, the pore fluid becomes over-pressured during decompression and additional fluid is generated due to pressure re-equilibration (Staude et al., 2009).

In the NPO, the Alston Block is underlain by the Weardale Granite (Holland and Lambert, 1970) and the Askrigg Block is underlain by the Wensleydale Granite (Bott and Smith, 2017; Fig. 1; Dunham et al., 1968; Webb and Brown, 1989). Already in the mid-1960s, Sawkins (1966) indicated that fluorine and at least some base metals in the mineralization in the NPO may have originated from a deep-seated magmatic source. Some contribution in the form of either heat, metals and/or chemicals from a granitic batholith towards the mineralization in the NPO is assumed for the fluorite mineralization in the Alston Block, but further south in the Askrigg Block, there is no information on any potential contribution of the Wensleydale Granite towards the Askrigg mineralization (Bott and Smith, 2017).

In this contribution we aim to provide a better understanding of the origin of fluorite veins and their potential genetic relation to basement granites. Here, we show that the fluorites from the two blocks in the North Pennine Orefield are markedly different in their REY concentrations, their Sr- and Nd isotope geochemistry and in their fluid inclusion compositions, albeit both blocks are underlain by coeval basement granites of similar composition.

2. Geological setting

2.1 The Northern Pennine Orefield

The Pennines are a ca. 400km long mountain range in Northern England. The Pennine Orefield is subdivided into the Northern Pennine Orefield (NPO) and the Southern Pennine Orefield (SPO; Fig. 1). The NPO itself is subdivided into two fault-bounded crustal blocks; the Alston Block, which comprises the northern part of the NPO, and the Askrigg Block, which makes up its southern part (Dunham, 1990; Dunham and Wilson, 1985; Fisher et al., 2013). Figure 1 shows a simplified geological map that indicates the extents of the Northern and the Southern Pennine Orefield as well as the two studied crustal blocks of the NPO. In both blocks, the ca. 360-300 Ma old Carboniferous marine sedimentary strata that hosts the mineralization is underlain by granitic basement (Table 1; Fig. 1). The Alston Block is underlain by the Weardale Granite (Holland and Lambert, 1970) and the Askrigg Block is underlain by the Wensleydale Granite (Bott and Smith, 2017; Dunham et al., 1968; Webb and Brown, 1989). Both batholiths were emplaced in the Early Devonian (400 Ma) and are very similar in composition and origin (see Table 1). The upper parts of the two granites are weathered and Carboniferous sedimentary successions unconformably overlay the two batholiths (Webb and Brown, 1989). For a detailed petrologic description of the basement granites in the Pennines, see Webb & Brown (1989).

The Alston and Askrigg blocks constitute the structural highs of an anticline which is oriented north-south and the fault-bounded blocks represent areas of uplifted crustal parts of a basin-and-range system, with the two blocks separated by the Stainmore Trough (Evans et al., 2002). The Alston Block is bound to the north and south by the Stublick and Lunedale faults, which extend into the Northumberland Basin in the north and the Stainmore Trough in the south. Dolerites of Permian age (295.6 Ma; Fitch and Miller, 1967) intruded into the Carboniferous-Permian boundary layers in the Alston Block (the *Whin Sills*; Fitch and Miller 1967; Bott and Smith 2017). The Askrigg Block is bordered at its southernmost part by the Craven Fault (Fig. 1), which also separates the Askrigg Block and the NPO from the SPO. The bedrock comprises mostly Upper Carboniferous limestone and

Millstone Grit, a coarse-grained Carboniferous sandstone. The covered Wensleydale Granite, encountered only in drill core (Dunham, 1974), underlies the Askrigg Block in an east-west directed trend.

2.2 Mineralization

Fluorite-bearing MVT mineralization is described in the Alston (Bouch et al., 2008) and Askrigg Blocks (Bouch et al., 2006) of the NPO as well as in the SPO (Bau et al., 2003; Ford and Worley, 2016). Lead-Zn-F-Ba mineralization in the Alston Block is present as mostly hydrothermal fissure-vein infills and stratabound metasomatic replacement accompanied by brecciation and dissolution of Carboniferous limestones (Bevins, 2010; Bouch et al., 2008). The mineralization is characterized by a concentric zoning from early fluorite-quartz-sulphide to later stage barite mineralization, which may represent waning stages of the hydrothermal circulation system at lower temperatures (Bouch et al., 2006; Cann and Banks, 2001). Mineralization in the central fluorite zone is regarded to have been formed from high-salinity brines with fluid temperatures ranging up to 200°C and with cooler temperatures of 120°C measured towards the margin of the fluorite zone (Dunham, 1990; Sawkins, 1966). Fischer et al. (2013) indicate that the Weardale Granite may have exerted a certain structural control on the emplacement of orebodies present in the Alston Block. According to fluid inclusion data from Cann and Banks (2001), the granite, at approximately 300°C at that depth, heated highly saline, basinal brines derived from overlying Zechstein units to temperatures of about 200°C and focused the fluid flow in the sedimentary basin by heat convection. Kimbell et al. (2010) point towards a significant contribution of the deeply-covered Weardale Granite to the mineralizing fluids in the NPO. The location of the batholith apparently played an important role in channeling the hydrothermal fluid into the overlying Carboniferous strata. However, with regard to the discrepancies in suggested ages between granite (Dunham, 1974; 400 Ma; Holland and Lambert, 1970) and mineralization (250-260 Ma, 210 Ma; Cann and Banks, 2001; Davison et al., 1992; Dunham et al., 1968; Shepherd et al., 1982), a significant heat contribution of the granite towards the fluids and the mineralization is unlikely. Therefore, the discussed heat contribution is purely related to the

depth of the basement granite and the geothermal gradient; it appears likely that the Wensleydale granite in the Askrigg Block had a similar influence.

In the Askrigg Block, hydrothermal Pb-Zn-F-Ba mineralization occurs as stratabound deposits and as ribbon veins emplaced in faults with only minor displacement. In the Swaledale region, Pb-F-Ba deposits occur in fissure veins while vein mineralization of galena and fluorite is present in the southern portion of the Askrigg Block. Copper-bearing veins were described from the eastern and western flanks of the Askrigg Block (Bevins, 2010), but the zonal distribution is less well understood than in the Alston Block (Bevins, 2010). The general distribution of veins and mineral occurrences does not reflect the underlying Wensleydale Granite, which is in marked difference to the mineralization above the Weardale granite in the Alston Block. However, it was suggested that it may have exerted a certain structural control on sedimentation and tectonics in the area (Ineson, 1976; Small, 1977).

In the Pennine Orefield, deep-seated, moderately acidic, highly saline NaCl-$CaCl_2$ brines carrying hydrocarbons, Pb, Zn, F and Ba, were transported into Carboniferous platform carbonates, where the mineralization formed due to acid neutralization and sulfate reduction (Plant et al., 1988). Sulphur and oxygen isotope data imply that the fluids, or at least the sulphur and oxygen contained in these fluids, were mostly derived from basinal brines (Crowley et al., 1997; e.g., Solomon, 1966; Solomon et al., 1971), supporting the hypothesis that mineralization has an MVT affinity. In the following decades, numerous studies on fluorite mineralization in the NPO and SPO were published. These included studies on trace elements (Bau et al., 2003; Shepherd et al., 1982), fluid inclusions (Bouch et al., 2008, 2006; Cann and Banks, 2001; Ewbank et al., 1995; Plant et al., 1988; Sawkins, 1966) as well as stable isotopes and radiometric dating (Bau et al., 2003; e.g., Jones and Swainbank, 1993).

Fluorite mineralization in the NPO has been tentatively linked to crustal subsidence and declining geothermal gradients, where Viséan-Namurian shale basins dewatered and the system was overpressurized due to seismic pumping related to early Permian tectonism (Plant et al., 1988).

Other studies suggest however, that the majority of the mineralization formed in two phases during the late Permian (Cann and Banks, 2001; Davison et al., 1992; 250-260 Ma; Dunham et al., 1968; Shepherd et al., 1982) as well as at the end of the Triassic (210 Ma; Cann and Banks, 2001). There is currently no data available that could clarify this discrepancy, however, studies on comparable MVT deposits in Europe suggest a significant age gap between host rocks and hydrothermal mineralization. Many of the epigenetic analogues in Europe are much younger than the Variscan orogeny and are thought to be related to the opening of the North Atlantic (170-180 Ma; Munoz et al., 2005; Staude et al., 2009).

3. Samples & methods

The mineral samples from the Alston and Askrigg Blocks that were studied in this contribution are listed in ESM Tables 1 and 2. The mineral specimens were collected from open workings in the respective underground or open-pit mines. Sample designations, grid reference numbers and sample localities are also shown in ESM Tables 1 and 2. The fluorite samples chosen for REY analysis were obtained from the NPO from various localities in the Alston Block (18 deposits) and the Askrigg Block (11 deposits), respectively. A subset of the fluorites from both blocks was also chosen for Sr- and Nd isotope geochemistry. The Alston Block fluorites are described in detail in Cann and Banks (2001). The fluorites are zoned but the growth zones are large (several mm-cm width) and only discrete zones were sampled in the course of this study. The minerals precipitated in monomineralic form. Close intergrowth of fluorite and quartz is not common. An exception is at Frazer's Hushes mine (ESM Table 2) where 5-10 cm thick bands of different generations of fluorite precipitated on each other as big well-formed cubes with ca. 1cm thick intermittent bands of quartz.

3.1 Fluid inclusion microthermometry and crush leach analysis

Doubly polished 200-300µm thick wafers of quartz, fluorite and barite were used to determine fluid inclusion petrography and to determine the salinity, homogenization temperature and bulk

composition. Phase transitions in fluid inclusions were measured using a Linkam THMS 600 heating freezing stage calibrated with synthetic fluid inclusions and salts of known melting point. The accuracy of measurements below 0 °C was ± 0.2 °C and above 100° C was ca. ± 2 °C. The precision of low temperature phase transition measurements was ± 0.1 °C and ± 1.5 °C for the temperature of homogenization.

Samples chosen for crush-leach analysis had previously been studied by microthermometry to ensure that they contained a single dominant fluid population either in terms of numbers of inclusions or salinity. In all of these samples inclusions were dominated by high salinity fluids. Barite was a notable exception where there was also a small number of inclusions of low salinity present. These low salinity inclusions will only cause a minor error due to contamination and the data from barite is thus reliable for the higher salinity fluid. Fluorite, quartz, barite, sphalerite and calcite mineral separates were crushed to 1-2mm in size and cleaned prior to analysis using the procedure described in Banks et al. (2000). In fluorite where there were different periods of large crystal growth, samples were taken from within individual growth bands, which in many cases were 10's of mm wide. Fluorite, barite and quartz were cleaned in hot aqua-regia prior to repeated washing in boiling 18.2 MΩ water. Calcite and sphalerite were cleaned by repeated boiling in 18.2 MΩ water. After drying, the minerals were crushed to a fine powder in an agate pestle and mortar, transferred to a Sterilin sample container and 7ml of 18.2 MΩ water were added to dissolve the contents of the opened fluid inclusions that had dried on the mineral. The contents were filtered through a 0.2µm nylon filter to remove any particulates prior to analysis. Anions were determined with a Dionex DX500 ion chromatograph and cations by atomic emission spectroscopy (AES). Detection limits were; Cl ~ 25ppb, Br ~1ppb, SO_4 ~10ppb, Na, K ~20ppb and Li ~ 0.1ppb. The precision, based on replicate analysis of the same leach solutions, was less than 5% RSD for ion chromatography and 4% RSD for AES. The anion and cation concentrations, as analysed, are given in ESM Tables 1 and 2 and Na/Br and Cl/Br molar ratios are plotted in Figs. 2a and 2b, respectively.

3.2 Rare earth elements and Yttrium

All rock samples were thoroughly rinsed with de-ionized water and dried before further treatment. The rock samples were then crushed to a particle size of 2-10 mm and fluorite grains were hand-picked in order to minimize contamination by host rock or other minerals. Fluorite separates were milled in agate mortars using a Fritsch Pulverisette 6 planetary ball mill to a fine-grained powder with <64 µm grain size. For bulk rock decomposition, a Picotrace DAS acid digestion system (Picotrace GmbH, Bovenden, Germany) was used. All acids used in this study for decomposition of sample material and analysis were of suprapur grade and purity of all reagents was verified by blank measurements. The mineral powders were dried at 110°C for 24 hours before an aliquot of ca. 0.3g was put into acid-cleaned PTFE digestion vessels and digested with a mixture of 1 ml concentrated HF, 1 ml concentrated HCl and 3 ml concentrated HNO_3 for 12 hours at 200 °C and afterwards evaporated to incipient dryness. The samples were treated for another 72 h with 3 ml of concentrated HF and 3 ml of concentrated $HClO_4$ at 200 °C and subsequently evaporated. Dulski (2001) and Alexander (2008) outline details of the digestion procedure and on analytical precision of the employed analytical techniques. After digestion, the samples were taken up in 20 ml of a mixture of 0.5M HNO_3 and 0.01M HF. The digested bulk rock samples were analysed with a Perkin-Elmer quadrupole ICP-MS ELAN drc-e for Ba, Sr and rare earth elements and Y (REY). Background intensities of procedural blanks were at least two orders of magnitude lower than sample intensities for the studied elements. Certified reference material as well as sample duplicates were used in order to estimate reproducibility of the applied analytical technique and for quality assurance. Accuracy of the ICPMS measurements was monitored by analysing the CRM standards JLs-1 (carbonate), J-Do1 (dolomite), BHVO-2 (basalt) and IF-G (iron formation) as well as procedural blanks. Rare earth element and Y concentrations of the CRM standards obtained with ICPMS are within rel. 5% deviation from published literature values (Dulski, 2001).

3.3 Calculation of REY_{SN}, Ce_{SN}/Ce^*_{SN} and Eu_{SN}/Eu^*_{SN} anomalies

Rare earth element and yttrium concentrations are normalized to European Shale (EUS; Bau et al., 2018) in Figs. 3a-c and Fig. 5. In this contribution, normalized data are referred to as REY_{SN}, the subscript indicating that data are normalized to shale. Rare earth element anomalies are calculated based on EUS-normalized data using the equations of Bolhar et al. (2004) for Ce_{SN}/Ce^*_{SN} and Bau (1996) for Eu_{SN}/Eu^*_{SN} as follows:

Equation 1:

$$\frac{Ce_{SN}}{Ce^*_{SN}} = \frac{Ce_{SN}}{(2 * Pr_{SN} - Nd_{SN})}$$

Bolhar et al. (2004)

Equation 2:

$$\frac{Eu_{SN}}{Eu^*_{SN}} = \frac{Eu_{SN}}{(0.67 * Sm_{SN} + 0.33 * Tb_{SN})}$$

Bau (1996)

Deviations from unity reveal decoupling of redox-sensitive Ce and Eu from their strictly trivalent REY neighbours La^{3+} and Pr^{3+} for Ce and Sm^{3+} and Tb^{3+} for Eu. Ratios of >1 and <1 indicate positive and negative anomalies, respectively.

3.4 Sr-Nd isotope geochemistry

Sample splits from the trace element analyses of four Askrigg Block fluorites, six Alston Block fluorites and the certified reference materials JDo-1 (issued by Geological Survey of Japan) and IF-G (issued by Centres de Recherches Petrographiques et Geochimiques) were analyzed for Sr-Nd isotopes at the Department of Lithospheric Research (University of Vienna) using ion exchange column separation chemistry and thermal ionization mass spectrometry (TIMS). Circa 50 mg to 200 mg of the powders were digested in an ultrapure acid mixture of concentrated HF-HNO_3 (4:1) for two weeks at 130 °C. The solutions were evaporated, treated with 2ml conc. HNO_3 and subsequently

dried down to incipient dryness. An additional treatment with 8ml conc. HCl and subsequent evaporation was performed before re-equilibration in 2ml 2.5N HCl. The following ion exchange column chemistry and Sr-Nd isotope measurements via Re double filaments with a Thermo Finnigan Triton TI TIMS are described in detail elsewhere (Wegner and Koeberl, 2016). The international standards NBS987 and La Jolla yield $^{87}Sr/^{86}Sr$ of 0.710260 ±3 (n=8) and $^{143}Nd/^{144}Nd$ of 0.511839±6 (n=7); respectively; maximum blanks are below 1 ng for Sr and below 50 pg for Nd. Mass fractionation during TIMS measurements was corrected with $^{88}Sr/^{86}Sr$ = 8.3752 and $^{146}Nd/^{144}Nd$ = 0.7219. $^{87}Sr/^{86}Sr$ of CRM JDo-1 was 0.512248±5 and $^{143}Nd/^{144}Nd$ was 0.707548±5, whereas $^{87}Sr/^{86}Sr$ of CRM IF-G was 0.511379±6 and $^{143}Nd/^{144}Nd$ was 0.719517±6 (see ESM table 6).

4. Results & Discussion

4.1 Fluid inclusion petrography and microthermometry

Fluid inclusions were measured from fluid inclusion arrays (FIA's) that represented primary or pseudosecondary inclusions. In fluorite, many of the FIA's were obviously aligned along the crystal growth faces and as fluorite exhibited discrete periods of crystal growth these were particularly prevalent. In quartz, fluid inclusions were less numerous but again were clearly of primary origin.

In fluorite, quartz and barite inclusions were L-V; barite also contained a certain number of L-only inclusions. Barite is particularly susceptible to stretching, either during heating or sample preparation, which induces the formation of vapour bubbles in inclusions that should only contain liquid as they represent low temperature fluids (Ulrich and Bodnar, 1988). Yet, we suggest that barite contains two generations of fluid inclusions trapped at different temperatures and with different salinities. This suggestion is based on textural relations in FIA's and the observation that the salinity in L-only inclusions is much lower compared to that recorded in L-V inclusions. Where possible the following phase changes were measured in the samples: T_e: eutectic temperature, T_{hyd}: hydrohalite dissolution temperature, T_{ice}: final ice melting temperature and T_h: homogenization temperature of

the L-V inclusions to liquid. On freezing the majority of the inclusions turned a brown colour indicating the presence of a significant Ca concentration in the fluid.

The temperatures and salinities for the Alston and Askrigg Block mineralization as obtained from fluid inclusion assemblages (FIA) are provided in ESM Table 3. FIA in Alston Block fluorite, quartz, calcite and barite are rather uniform with homogenization temperatures between 105-160°C (104-134°C for calcite) and fluid salinities ranging between 18.4-22.7 % wt% NaCl equiv. FIA from Askrigg Block show similar homogenization temperatures in the range of 99-173°C, but a significantly larger range in fluid salinities (12.4-26 wt% NaCl equiv).

The low eutectic melting temperatures and the fact that the inclusions go brown on freezing indicate a significant concentration of $CaCl_2$ in addition to NaCl in the fluids. Using the pairs of hydrohalite and ice melting temperatures it is possible to estimate the Ca/Na ration in the fluid inclusions. The ice and hydrohalite melting temperatures are close to the eutectic value for the pure H_2O-NaCl system and therefore Na is still the dominant cation in the fluid. The estimated Ca/Na ratio is on average 0.3. This ratio is similar to the ratio of Ca/Na obtained from crush-leach (see below) and bulk analyses of a few monomineralic quartz mineral separates from the Alston Block. In general, the fluid characteristics are very similar for the inclusions in the different minerals from the Alston Block, while in the Askrigg Block there is more variability in salinity and temperature with lower salinities and higher temperatures reported compared with Alston.

4.2 Crush-leach analysis of fluid inclusions

The use of fluid inclusion analyses to determine fluid sources and processes relies on the anion composition (Cl and Br) behaving as essentially conservative components in aqueous fluids. Chlorine and Br have much greater concentrations in fluids than in minerals and water-rock interaction (WRI) does not alter their concentration, as they do not readily incorporate into newly formed minerals. In contrast, the cations in the fluid may be extensively altered by WRI processes. Here we are concerned primarily with the conservative anions as the minerals hosting the fluid inclusions

(fluorite, barite and calcite) all contain elements that would interfere in interpreting the cation compositions. In Na/Br and Cl/Br diagrams (Figs. 2a&b), the position of evaporating seawater does not change, despite increasing salinity by almost a factor of ten, until halite saturation is reached and salt precipitates. As Br is not readily incorporated into the halite structure it increases significantly in solution as halite precipitation proceeds leading to decreases in both the Na/Br and Cl/Br ratios in the fluid. Fontes and Matray (1993) provide a detailed analysis of the composition of seawater as evaporation proceeds through the sequence of different salts that precipitate. Fluid inclusions that plot on or close to the evaporation trend, drawn from the above-mentioned data, would indicate little or no WRI to exchange cations in the fluid with cations either along the flow path or at the site of mineral deposition.

Based on Na/Br and Cl/Br molar ratios from the fluid inclusions as shown in Fig. 2a and reported in ESM Table 1, the Alston Block minerals studied here fall into three main groups. All quartz and barite samples have the same range of ratios and plot on the line that represents seawater evaporation past halite saturation. These are Br-rich bittern brines (residual fluids after seawater has been evaporated past halite saturation) associated with evaporite deposits and should, for this degree of evaporation, have salinities in the range of c. 25-30 wt% NaCl equiv. However, the salinities in the fluid inclusions are >c. 20 wt% NaCl equiv, which indicates a significant dilution by a low salinity fluid. In fluorite, the majority of samples fall into two groups. The first group clusters around the values for seawater (n=4) and a further three fluorites and one sphalerite in this group have the same Cl/Br ratio as seawater but have lower Na/Br ratios. The latter are indicative of Na loss from the fluids, usually in exchange for Ca. The second group of fluorites have Cl/Br ratios much higher than seawater, which indicates a certain contribution from dissolution of halite. These fluorites also have a large reduction in the Na/Br ratio, indicative of loss of Na by either albitization of plagioclase and release of Ca into the fluid or by mixing with Ca-rich fluids. The fluid inclusions in quartz, barite and parts of the fluorites show little evidence of loss of Na through fluid-rock interaction whilst other

fluorites do. This indicates that there were multiple sources of fluids contributing towards the mineralization found in the Alston Block.

ESM Table 2 and Figure 2b show the results of the crush-leach analysis conducted on fluorites and gangue minerals from the Askrigg Block. The element ratios in the different minerals are less variable when compared to those in the Alston Block. Here, the different minerals, except calcite in the shaded ellipse, plot close to seawater and, like the minerals studied from the Alston Block, plot along the trend for seawater that has evaporated past halite saturation. There is less loss of Na from the fluids compared with those in the Alston Block. The fluid inclusion data indicates that fluorite here is derived from the same fluid as quartz and barite, while in the Alston Block the majority of fluorite is from a quite different fluid source. This observation can also be made in the REY geochemistry and the Sr-Nd isotope signatures of the investigated fluorites (see below). The fluid inclusions in calcite have the same Cl/Br ratio as fluid inclusions in the other minerals, but have much greater Na/Br ratios, plotting to the right of the 1:1 line (Fig. 2b). It needs to be stressed here that calcite is paragenetically later than the other minerals studied here.

The microthermometry data indicate there is significant Ca in the fluid inclusions. For seawater that has evaporated to these high salinities there should be none (Fontes and Matray, 1993). The composition would be dominated by Na, Mg and K, but in many contemporaneous brines (Carpenter et al, 1974) and fluid inclusion analyses Na-Ca-Cl dominated fluids have been identified (Grandia et al., 2003; Heijlen et al., 2003, 2001; McCaig et al., 2000; Piqué et al., 2008). Davidson and Criss (1996) suggest that the excess Ca in fluids arises from albitization of plagioclase and the exchange of Na for Ca in a 2:1 ratio. However, if this were the sole cause of increased Ca then the fluids would still have significant Mg but they do not. If the increasing Mg as seawater is evaporated reacts with limestone to produce dolomites, then on their excess-deficit plot the fluids would lie along the same 2:1 line. Dolomitization is common in the North Pennine Orefield as it is in other similar carbonate areas with low temperature fluorite and base-metal mineralization.

The halogen data shown in ESM Tables 1 and 2 and Figs. 2a-b and discussed above show that there are multiple fluid types and therefore most likely also multiple fluid sources involved with the mineralization in both the Alston and Askrigg Blocks. There also appears to have been different degrees of modification of these fluids by fluid-rock interactions. This is most obvious in fluorite from the Alston Block where the fluids have experienced a significant loss of Na and an increase in Ca, probably from (hydrothermal) albitization of plagioclase. According to Bouch et al. (2006), the mineralization in the Alston Block was caused by mixing of several low-salinity fluids such as sodic groundwater with high-salinity calcic brines that carried elevated metal contents. Here we suggest that there were at least three different fluid sources involved; (i) a fluid of unknown source that dissolved halite, (ii) seawater that evaporated to high salinity but not past the point of halite precipitation and (iii) Br-rich bittern brines which could be residual fluids after seawater evaporation past halite saturation (i.e., Walter et al., 2016) and which was diluted by a low salinity fluid, potentially originating from the basement. The data represents different fluids entering the orefield at different times. A mixing process of bittern brines with halite dissolution brines was also described in a study on continental basement brines from the Schwarzwald in Germany (Walter et al., 2016). With two exceptions, all fluids in fluorite involve evaporated seawater or a component from dissolution of halite. The two exceptions are AL96-24 (Hilton Mine) and AL96-26 (Cambokeels Mine), for which halogen contents are more indicative of Br-rich bittern fluids. Experimental results showed that fluid-rock interaction is insufficient for the production of brines with similar high salinities and low Cl/Br ratios (Burisch et al., 2015). According to Walter et al. (2016), external fluid sources are therefore required. In addition to the basinal brines, the Zechstein facies is present close to the mineralized zones and could represent a potential external fluid source as evidenced by evaporite minerals and high Br concentrations in the fluids (Cann and Banks 2001).

4.3 REY geochemistry

Fluorites from the Alston Block in the northern part of the NPO are characterized by elevated total REY concentrations ranging from 173 mg kg^{-1} to 923 mg kg^{-1} with average concentrations of 553 mg

kg^{-1} ΣREY (n=16; ESM Table 4). The REY$_{SN}$ patterns shown in Fig. 3a indicate an enrichment of the middle REY (MREY: Sm-Dy) over light (LREY: La-Sm) and heavy REY (HREY: Gd-Lu) with Y/Ho fractionation observed in all Alston hydrothermal vein fluorites. Noteworthy is a distinct fractionation of Eu in all but two Alston Block samples, resulting in positive Eu$_{SN}$ anomalies with Eu$_{SN}$/Eu$^*_{SN}$ ratios in the range between 2.68 and 8.87, positive La$_{SN}$ anomalies but lack of Ce$_{SN}$ anomalies. The only exceptions are, as with the fluid inclusions, samples AL96-24 (Hilton Mine) and AL96-26 (Cambokeels Mine). Both of these lack anomalous behaviour of Eu (Eu$_{SN}$/Eu$^*_{SN}$: 0.79 and 1.11, resp.), but do show similarly elevated total REY concentrations. This may indicate the involvement of an additional (Br-rich) fluid source and may also point to different pathways and fluid sources for fluorite mineralization in the Cambokeels and Hilton mines in relation to the mineralization at the other Alston sites.

The total REY concentrations in fluorites from localities in the Askrigg Block in the southern part of the NPO are considerably lower than those observed in fluorites from the Alston Block (ESM Table 5). Total REY concentrations range from 21.6 to 68.7 mg kg^{-1} and are on average 42.7 mg kg^{-1} (n=8), i.e. more than ten times lower than those found in Alston Block fluorites. The REY$_{SN}$ patterns, however, show a similar enrichment of MREY over both LREY and HREY (Fig. 3b). The depletion of LREY relative to MREY is exceptionally strong and covers about two orders of magnitude in the shale-normalized patterns. All samples show Y-Ho fractionation, i.e. positive Y$_{SN}$ anomalies, but lack any Eu$_{SN}$ anomalies (Eu$_{SN}$/Eu$^*_{SN}$ = 0.99 - 1.33). The Askrigg Block fluorites also show small negative Ce$_{SN}$ anomalies with Ce$_{SN}$/Ce* as low as 0.93, positive La$_{SN}$ anomalies, and enrichment of Gd$_{SN}$ relative to Tb$_{SN}$ and Dy$_{SN}$.

The REY$_{SN}$ patterns differ considerably between the Alston Block in the northern part of the NPO and the Askrigg Block in its southern part. However, the patterns are rather consistent within each area and between the respective individual sites. Distribution and hence transport of the REY in the individual blocks was, therefore, not controlled by a specific proximity to faults and other structural features. Bau et al. (2003) studied the REY geochemistry of fluorites from the Southern Pennine

Orefield and fluorites from the Frazer's Hushes Mine in the Northern Pennine Orefield. While the Frazer's Hushes fluorites match well with the fluorites from the Alston Block discussed in our study, the REY_{SN} patterns of the Askrigg Block fluorites in the NPO more closely resemble fluorites from the SPO (Bau et al., 2003). Bott and Smith (2017) published mean La, Ce and Y concentrations of fluorites from the Alston Block (referred to as 'North Pennines') and the Askrigg Block. Their data were obtained by x-ray fluorescence spectrometry, but compare well to the REY data presented in our study.

All fluorite samples investigated in this study show a distinct fractionation of Y from its geochemical twin Ho (Fig. 4). Ratios of Y/Ho range from 42 - 97.4 in fluorites from the Alston Block and 97 - 154 in Askrigg Block fluorites. Such superchondritic Y/Ho ratios are a common feature of many fluorite occurrences worldwide (e.g., Bau and Dulski, 1995; Graupner et al., 2015). Yttrium is significantly enriched in fluorite, probably due to the significantly higher stability constants of Y fluoride complexes relative to Ho fluoride complexes in hydrothermal solutions (Bau, 1996; e.g., Bau and Dulski, 1995). It is noteworthy that (i) Askrigg Block fluorites show significantly higher Y/Ho ratios than Alston Block fluorites and (ii) the Viséan limestones which host the mineralization in the SPO, also have elevated Y/Ho ratios (Bau et al., 2003). Such positive Y_{SN} anomalies are common in detritus-poor marine sedimentary carbonates and seawater (Bau et al., 1999, e.g., 1995; Schier et al., 2018). Therefore, hydrothermal fluids which mobilized REY from the marine limestones in the Askrigg Block started with much higher Y/Ho ratios than those circulating in the Alston Block. The different extents of Y-Ho fractionation observed in NPO fluorites can, therefore, be attributed to different REY sources.

The low solubility of REY-fluorides imposes a limitation on transport of the REY as fluoride complexes. Hence, in hydrothermal solutions, REY are more likely to be transported as chloride complexes (Migdisov and Williams-Jones, 2014). Dissolution of the carbonate host rocks by aqueous fluids causes a rapid increase in pH, possibly liberating Ca ions to the fluid and allowing for subsequent deposition of fluorite (Rajabzadeh, 2007) along with parts of the REY that are dissolved in these fluids. The fluoride ion in this case acts as a binding ligand for REY deposition along fluorite

mineralization but does not act as a complexing ligand (Migdisov and Williams-Jones, 2014). The source of fluorine within fluorite-rich subtypes of MVT deposits, however, is still under discussion. Models for fluorite genesis in the Illinois-Kentucky district in North America propose the mixing of magmatic fluids with sedimentary brines (Plumlee et al., 1995). The REY_{SN} patterns (Fig. 3a-b) as well as the contrasting total REY concentrations and Y-Ho fractionation in fluorite indicate that the fluids from which these hydrothermal fluorites formed had experienced different physico-chemical environments, particularly with respect to temperature and REY sources.

Potential causes for Eu_{SN} anomalies in hydrothermal minerals

The Alston Block fluorites show positive Eu_{SN} anomalies, indicating the decoupling of redox-sensitive Eu from its strictly trivalent REY neighbours. In marked contrast, Eu_{SN} anomalies are altogether missing in Askrigg Block fluorites (Fig. 5) and in SPO fluorites (Bau et al., 2003). Either of the following three mechanisms (or a combination these) may cause Eu anomalies in normalized patterns (Eu_N) of hydrothermal vein minerals and fluids:

(a) *Inheritance*: the Eu_N anomaly in the studied mineral/fluid could be inherited from the source rock or any rock that the fluid leached during its evolution and that carried significant amounts of REY. This implies that one of the rocks that interacted with the fluid should show such an anomaly. Lithologies showing positive Eu_{SN} anomalies in shale-normalized REY patterns are mafic and ultramafic rocks such as basalts and peridotites. However, neither are such (ultra)mafic rocks abundant in the NPO, nor would they display positive Eu_{SN} anomalies as large as those observed in the fluorites.

Geochemical data for the Weardale and Wensleydale granites are scarce and only incomplete REY data are reported by Webb & Brown (1989). The REY_{SN} patterns are plotted in Fig. 3c along with those for the Whin Sill dolerite, which is available as the CRM "WS-E" for which excellent analytical data are available from Govindaraju et al. (1994) and numerous other sources. Comparison of the REY_{SN} patterns in Figs. 3a-c shows that neither of the three igneous rocks occurring in the NPO bears

any similarity to the patterns obtained for the fluorites studied here. The Weardale Granite, in contrast to the Alston fluorites, does not show a Eu_{SN} anomaly, the Wensleydale granite in the Askrigg Block has a negative one, and the Whin-Sill dolerite in the Alston Block shows an only small positive anomaly.

(b) *Selective mineral alteration or partial rock dissolution: l*eaching or alteration of a certain mineral or portion of a rock that carries significant amounts of Eu (e.g., feldspars due to substitution of Ca^{2+} by Eu^{2+}) relative to other MREY or that is depleted in Eu relative to other MREY, i.e. due to fractional crystallization. In basalts and basaltic andesites, the melt in the vicinity of a growing plagioclase crystal becomes selectively depleted in Eu due to preferential partitioning of Eu^{2+} into the crystal lattice of plagioclase. This may lead to REY_N patterns with negative Eu anomalies at grain boundaries, in the groundmass and in the interstitial spaces of the minerals (Giese and Bau, 1994; Kraemer et al., 2015). These minerals, or the matrix, can be preferentially dissolved - or preferentially *not* dissolved - during water-rock interaction and selective leaching (see e.g., Kraemer et al., 2015), creating fluids that are either enriched - or depleted – in Eu relative to its strictly trivalent REY *neighbours* (Bach and Irber, 1998; Bau et al., 1998; Giese and Bau, 1994; Shibata et al., 2006). Eu_N anomalies in solutions can also form during short-term water-rock interaction with gneisses, but were not observed in similar leaching experiments with granites (Dill et al., 2011; Schwinn and Markl, 2005). Therefore, Eu_N anomalies in Alston fluorites are not inherited from water-rock interaction with granites or its constituents.

(c) *Temperature*: positive Eu_N anomalies are usually observed in modern acidic and reducing hydrothermal fluids with temperatures exceeding 200-250°C, such as in modern black smoker fluids from Mid-Ocean Ridges (e.g., Bau and Dulski, 1999). The Eu^{3+}/Eu^{2+} redox potential in aqueous solutions depends mainly on temperature and to lesser extents on pressure, pH and the speciation of the REY (Bau, 1991; Bau et al., 2010; Bau and Möller, 1992; Schmidt et al., 2010; Sverjensky, 1984). In the case that positive Eu_N anomalies have developed in a hydrothermal fluid due to high temperatures and reducing conditions, this relative Eu enrichment will be inherited by any mineral

that precipitates from this fluid, provided that most of the Eu in the fluid *at the time of precipitation* is in an oxidation state that allows incorporation into the respective crystal lattice (i.e., Eu^{3+} for fluorite). Therefore, the temperature needs to be below ca. 200-250°C during mineral formation, i.e., in a physico-chemical environment when most of the Eu has been re-oxidized to Eu(III). In contrast to microthermometry, the Eu^{2+}/Eu^{3+} geothermometry is hence recording the highest temperature (>200-250°C) a hydrothermal fluid had experienced *prior to* mineral formation and not a mineral's formation temperature.

The observed positive Eu_{SN} anomalies, accordingly, indicate that a REY-enriched hydrothermal fluid in the Alston Block was heated to a temperature exceeding 250°C at some stage *prior to* fluid mixing and/or fluorite precipitation (Bau et al., 2003; Bau and Möller, 1992). The anomalies in Alston fluorites were then caused, for example, due to the presence of an external heat source, in contrast to fluorites from the Askrigg Block, which – similar to fluorites from the SPO (Bau et al. 2003) – lack significant Eu_{SN} anomalies and which, therefore, did not experience temperatures in excess of 250°C.

Potential REY sources

Bau et al. (2003) used REY_{SN} patterns and Sr-Nd-Pb isotope systematics to highlight significant differences in the metal sources and in the maximum temperature of the fluorite-forming fluids between MVT mineralization in the SPO and of the Frazer's Hushes Mine in the NPO (Alston Block). According to Bau et al. (2003), fluorites from the SPO (e.g., "Blue John" fluorite from Treak Cliff Mine) show REY distributions with negative Ce_{SN} anomalies and positive Gd_{SN} and Y_{SN} anomalies and relatively low total REY concentrations (~28 mg kg^{-1} ΣREY on average). Direct comparison with the REY_{SN} patterns of Viséan limestone country-rock from the Dirtlow open-pit (Fig. 3c) suggest that REY in fluorites from the SPO were locally remobilized from adjacent marine sedimentary carbonate rocks (Bau et al. 2003). These marine sedimentary carbonate rocks show typical seawater REY features which were transferred to the limestone upon precipitation from seawater (e.g., Tostevin et al. 2016). We emphasize that the fluorites from the Alston and Askrigg blocks have REY_{SN} patterns and specific REY features that show a striking similarity to those found by Bau et al. (2003; e.g., Figs. 3-5),

yet Alston Block fluorites are significantly enriched in REY relative to Askrigg and SPO fluorites. The Askrigg Block fluorites show specific seawater (limestone) signals in their REY compositions (i.e., La_{SN}, Ce_{SN} and Gd_{SN} anomalies, elevated Y/Ho ratios). The REY in the Askrigg Block fluorites originate from the same source as the REY in SPO fluorites and we suggest that the REY in Askrigg fluorites were mobilized from similar source rocks, most probably marine Carboniferous limestones. The lack of seawater REY features, the elevated REY concentrations and the lower Y/Ho ratios in Alston fluorites indicate REY mobilization from a different source.

4.4 Sr and Nd isotopes

In order to further constrain the origin of the metals and the fluids in both districts, the $^{143}Nd/^{144}Nd$ and $^{87}Sr/^{86}Sr$ isotope ratios of carefully selected fluorites of both blocks were measured and compared to literature values from Bau et al. (2003) for SPO fluorites and Viséan limestone host rock and from Govindaraju et al. (1994) for the Whin Sill dolerite. Neodymium isotope data are not available for the two basement granites and for Sr only *initial* $^{87}Sr/^{86}Sr$ ratios (t=400 Ma) of isochron calculations were provided by Holland & Lambert (Weardale: $^{87}Sr/^{86}Sr$= 0.706 +/-2; 1970) and Dunham (Wensleydale: $^{87}Sr/^{86}Sr$=0.7210+/-44; 1974). Unfortunately, no data were provided that would allow us to recalculate modern-day $^{87}Sr/^{86}Sr$ isotope ratios, hence a comparison with $^{87}Sr/^{86}Sr$ in the fluorites and assumptions on fluid mixing between the granites and other sources cannot be made.

The Sr-Nd isotope systematics of samples from the Alston and Askrigg blocks are shown in Figs. 6 and 7. For Nd isotopes, the Askrigg fluorites plot in a very narrow field in the range of $^{143}Nd/^{144}Nd$ = 0.511903 - 0.512007 (Table 6) and are much less radiogenic than the Alston Block fluorites, which also show a much wider compositional variation with more radiogenic $^{143}Nd/^{144}Nd$ = 0.512050 - 0.512541 (Table 6; Figs. 6 and 7). Nd isotope compositions are similar to SPO (0.512110±21 – 0.512215±11; Bau et al., 2003) and Askrigg fluorites, and also between the majority of Alston fluorites studied here (Fig. 7a). This observation may indicate a similar crustal REY source for these minerals. The data also suggest that Askrigg fluorites are less radiogenic than the SPO fluorites, but in

general Askrigg as well as most Alston fluorites plot in the same range as the Viséan limestones reported by Bau et al. (2003; Fig. 7a). The Nd isotope data, therefore, suggest that the REY in the Askrigg and (most of) the Alston fluorites were sourced from the same upper crustal REY source, i.e. Carboniferous limestones or shales. We emphasize that the ultimate source of REY in both limestone and shale is the upper continental crust and therefore both sediments have similar Nd isotopic compositions.

The Sr isotope ratios for Alston and Askrigg Block fluorites are markedly different and provide a deeper insight into potential metal sources. The Askrigg fluorites plot in a very narrow field in the range of $^{87}Sr/^{86}Sr$ = 0.710639 - 0.710813 (ESM Table 6) and are much less radiogenic than the Alston Block fluorites, which also show a much wider compositional variation with more radiogenic $^{87}Sr/^{86}Sr$ = 0.710751-0.713896 (ESM Table 6; Figs. 6 and 7). It is evident that neither Alston nor Askrigg fluorites exhibit Sr isotope ratios comparable to the values reported for the Viséan limestone host rocks (0.707992±8 – 0.708020±13) and the fluorites from the SPO (0.707007±7-0.708500±7) reported by Bau et al. (2003). Therefore, while the REY data suggest a certain relationship between Askrigg Block fluorites and SPO, the isotopic composition of Sr provides a different story due to a much more radiogenic character of the Sr isotopes in the Askrigg and Alston fluorites (Fig. 7b) compared to the SPO. The Sr isotopes, on the other hand, are also decoupled from Nd isotopes (Fig. 6 and 7b), implying different sources for REY and Sr in the fluorites. Alston as well as Askrigg Block fluorites are much more radiogenic in their Sr isotopic compositions than the Whin Sill dolerite (Govindaraju et al., 1994), the SPO fluorites, and the Viséan limestones (Bau et al. 2003). Based on the fluid inclusion and REY data reported in the previous chapters, marine sediments can be identified as a metal source. Strontium isotope ratios of the SPO fluorites and the limestone (Bau et al. 2003) plot in the Mississippian seawater array (Fig. 7b; Veizer 1989). The NPO fluorites (Alston and Askrigg) are much more radiogenic in Sr isotopes and plot above the seawater array. Therefore, we constrain that Sr in the NPO mineralization is sourced by variable portions of mixing between a seawater/carbonate rock source as one endmember and an unknown, much more radiogenic

(magmatic or aluminosilicate-rich/shale) source derived from upper crustal components with $^{87}Sr/^{86}Sr$ >0.71 as the other endmember (Fig. 7b). The contribution of the unknown source towards the fluid is increasing from Askrigg to Alston Block fluorites. The latter also show a much larger variety in Sr isotope ratios (Fig. 7b), indicating a greater and more variable degree of mixing.

4.5 Implications on fluid sources and fluid reconstruction

Penetration of brines into crystalline basement and the fluid circulation between the basement/cover interface near unconformities has been discussed widely and is assumed to be of major importance for the formation of MVT-like deposits (Boiron et al., 2010). Bouch et al. (2006) suggest that the elevated metal contents in the fluids of the NPO are probably the result of an interaction with the Weardale Granite, the Whin Sill dolerite and/or the Paleozoic basement. Based on mineral and alkali geothermometry and Eu_{SN} anomalies in fluorite, studies showed that the mineralisation in (parts of) the NPO derived from fluids which experienced maximum temperatures of at least 220°C-250°C (Bau et al., 2003; this study; Rankin and Graham, 1988; Shepherd et al., 1982; Vaughan and Ixer, 1980). The mineralization in the SPO, on the other hand, was sourced from mainly low-temperature basinal brines which were heated due to the geothermal gradient to significantly less than 200 °C to 250°C (preventing formation of a positive Eu_{SN} Anomaly) and which circulated in the basin due to heat convection and tectonic events. For the SPO, Plant et al. (1988) and Kendrick et al. (2002) pointed towards an origin of the ore-forming fluids from nearby shale-rich sedimentary basins such as the Edale and Widmerpool Gulfs, supporting the basin-dewatering model for MVT formation in the Pennines (Plant et al., 1988). Other models involve contribution from a brine that is derived from meteoric water and which infiltrated into the system during a late Carboniferous to early Permian unroofing of the system (e.g., Cann and Banks, 2001; Bouch et al., 2008). The most recent fluid inclusion studies from the Alston area (Bouch et al., 2006) and from Askrigg (Rogers, 1978) concluded that the fluids responsible for the mineralization were dominantly low temperature - high salinity brines. Bouch et al (2006) report homogenization temperatures between 80 and 150°C with salinities of 21 to 23 wt% NaCl equiv. and for Askrigg Rogers (1978) reports homogenization

temperatures between 90 and 160°C and salinities between 15 and 25 wt% NaCl equiv. Our fluid inclusion results confirm that fluorite precipitation occurred at T_h=108-158°C in Alston and T_h=99-160°C in Askrigg Block, notably lower than the maximum temperature recorded by Eu geothermometry. Our fluid inclusion data also indicate that a mixing of several different fluids, including a Br-rich bittern fluid, formed the mineralization in the North Pennine Orefield. The processes that lead to the formation of Br-rich bittern brines are widely debated (Burisch et al., 2016). Some authors suggest Cl and Br leaching from hydrous silicates and selective leaching of felsic minerals (Burisch et al., 2016; Markl and Bucher, 1998; Stober and Bucher, 1999) while others indicate that seawater evaporation (i.e. Zechstein-derived fluids in the NPO) or freezing is responsible for the formation of these fluids (Boiron et al., 2010; Herut et al., 1990). However, these brines could have contributed significantly towards the mineralization in the NPO. Burisch et al. (2016) found that Br is mostly bound to highly soluble phases in felsic minerals and that selective leaching of such phases causes lower Cl/Br ratios. Therefore, Br-rich bittern brines could have formed due to the deep penetration of the surface brines into the basement granite and the associated intense water-rock interaction due to heating of the fluids to temperatures >250°C.

The REY in the Askrigg Block and in the SPO were sourced from marine limestones. The higher REY concentrations and lower Y/Ho ratios observed in the Alston Block, however, demand for a different REY source. In the Alston Block, the REY data suggest that the basin-derived fluids were heated to higher temperatures than the fluids in the Askrigg Block and in the SPO. In fact, both the Weardale as well as the Wensleydale granite could have, due to the percolation of fluids, contributed heat and metals to the mineral system. Heat production of the two coeval granites was reported to be about equal (3.7 and 3.3-3.4 µW m-3; Webb and Brown, 1989) and current models explain the heating of the fluids in Alston mostly by the depth of the granite and the geothermal gradient (Cann and Banks, 2001). However, considering the similar situation in Askrigg, a comparable potential influence on the mineralization would be expected. REY concentrations of the two granites are also similar within one or two orders of magnitude (Webb and Brown, 1989). Therefore, the sole

presence of a granite at depth does not necessarily produce fluids with high REY contents, high temperatures and more radiogenic Sr. Instead, both granites probably acted as important pathways for the circulating fluids and maybe as a source for some fluid constituents, but higher temperatures and higher REY concentrations were only achieved in the Alston Block. Burisch et al. (2016) showed in alteration experiments with granites and gneisses that metals like Pb and Zn and halogens like F are readily released into the fluids with time and hence granites may represent potential metal sources for Pb-Zn-F-Ba mineralization. Judging from the REY concentrations, patterns and Sr-Nd isotope ratios, the Whin Sill dolerite did not contribute metals such as REY or Sr to the fluids in Alston. Bott and Smith (2017) indicated, however, that the 295 Ma old Whin Sill magma may have underplated the Weardale Granite in the Alston Block in some areas due to its higher density. This suggests that the high REY concentrations and the elevated temperatures in the Alston Block may be the combined result of the interaction of (at the time of formation) hot Whin Sill dolerite with the cold basement granite, which facilitated metal and/or heat transport for the mineralization that formed in the Alston Block. Here, REY were probably sourced from aluminosilicate-rich rocks, e.g., Lower Carboniferous shales, which were intensely leached due to the elevated fluid temperatures. Such an intrusion and hence underplating was not described for the Askrigg Block (Colman et al., 1989) which may well explain the different fluid sources and the lack of Eu_N anomalies in fluorites from this district.

Our neodymium isotope data suggests some similarity of Alston fluorite samples from Cambokeels (AL-24) and Hilton Mines (AL-26) to Whin Sill Nd isotopes (Fig. 6). These two fluorites also have elevated REY concentrations typical for Alston Block fluorites, but interestingly lack positive Eu_{SN} anomalies and show evidence of Br-rich bittern brines in their fluid inclusions. As indicated above, the Br-rich brines may point to water-rock interaction with hydrous silicates (Kullerud, 1996; Markl and Bucher, 1998). The differences in Eu_{SN} anomalies in certain fluorite specimens may indicate temperature heterogeneities in certain areas of the Alston Block. The fluids transported similarly high amounts of REY, but temperatures obviously were not high enough (<250°C) to enable

Eu fractionation within the fluid. The lower temperatures in some areas within the Alston Block are probably related due to mixing with cold residual surface brines as indicated by crush-leach data or markedly different fluid pathways due to structural relationships.

5. Conclusions

The Pennine Orefield hosts abundant fluorite mineralization that differs significantly between the Alston and Askrigg blocks in the NPO and between the NPO and SPO in general. While there are some initial similarities in geologic settings and in the fluid compositions as evidenced by fluid inclusions for all three areas, each area features apparently unique characteristics that modified and altered the fluid compositions. We showed that the REY systematics are very different between the two studied blocks and the source of REY are marine limestone (Askrigg) or shale (Alston). The maximum temperatures in Alston Block were >200-250°C, whereas fluids in Askrigg never experienced temperatures that high. This significant maximum temperature difference and different sources caused the differences in REY systematics, with higher REY concentrations and positive Eu_{SN} anomalies in Alston and about ten-times lower REY concentrations and lack of Eu_{SN} anomalies in Askrigg fluorites.

Mineralization of the Mississippi-Valley Type usually lack association with igneous activity (Colman et al. 1989). While the occurrences in the SPO represent varieties of MVT-style mineralization in a very classical sense (Dunham 1988; Plant 1988; Bau et al. 2003; Leach et al. 2005), we show that some of the fluid constituents for the NPO mineralization were sourced from the two Early Devonian basement granites. The unusually high temperatures observed in Alston are possibly related to a later dolerite intrusion (the Whin Sill) at around 295 Ma, which was also emplaced in and interacted with the (cold) basement granite. This also sets a tentative age constraint of ca. 295 Ma on the fluorite mineralization in the Alston Block.

A potential contribution from magmatic sources towards F-rich (MVT) mineralization is suggested for a range of European and North African deposits, such as those occurring in the Northwestern Massif Central, France (Boiron et al., 2010; Munoz et al., 1999, 1994), the Jebel Stah in Tunisia (Souissi et al., 2010), the Bohemian Massif in Germany (Dill et al., 2011) and the Central Pyrenees in Spain (Subías et al., 1998). In the Valle de Tena district in the Central Pyrenees, a fluorite generation is in contact with diabase dykes (Subías and Fernández-Nieto, 1995). These fluorites exhibit positive Eu_{SN} anomalies which were attributed to feldspar alteration (Subías and Fernández-Nieto, 1995), but which could also be explained by elevated maximum temperatures due to an interaction with the adjacent dyke. Fluorites that are not associated with dykes lack Eu_{SN} anomalies (Subías et al., 1998). The major difference to the Alston Block fluorites, however, is the about ten to hundred-fold lower concentration in total REE in the Valle de Tena fluorites (Subías et al., 1998).

6. Acknowledgments

We appreciate the help of E. Kurahashi and A. Moje in the Geochemistry Lab at Jacobs University Bremen, M. Horschinegg in the GeoKosmoChronology Lab at the University of Vienna, and R. Guest at the University of Leeds. S.V. partly received funding for this project from the European Union's Horizon 2020 research and innovation program of the Marie Sklodowska-Curie grant agreement No. 746033 for project ELEMIN.

7. References

Alexander, B.W., 2008. Trace element analyses in geological materials using low resolution inductively coupled plasma mass spectrometry (ICPMS) Technical Report No . 18 School of Engineering and Science. Jacobs University Bremen.

Bach, W., Irber, W., 1998. Rare earth element mobility in the oceanic lower sheeted dyke complex: evidence from geochemical data and leaching experiments. Chem. Geol. 151, 309–326.

doi:10.1016/S0009-2541(98)00087-4

Banks, D.A., Giuliani, G., Yardley, B.W.D., Cheilletz, A., 2000. Emerald mineralisation in Colombia: fluid chemistry and the role of brine mixing. Miner. Depos. 35, 699–713. doi:10.1007/s001260050273

Bau, M., 1996. Controls on the fractionation of isovalent trace elements in magmatic and aqueous systems: evidence from Y/Ho, Zr/Hf, and lanthanide tetrad effect. Contrib. to Mineral. Petrol. 123, 323–333.

Bau, M., 1991. Rare-earth element mobility during hydrothermal and metamorphic fluid-rock interaction and the significance of the oxidation state of europium. Chem. Geol. 93, 219–230. doi:10.1016/0009-2541(91)90115-8

Bau, M., Balan, S., Schmidt, K., Koschinsky, A., 2010. Rare earth elements in mussel shells of the Mytilidae family as tracers for hidden and fossil high-temperature hydrothermal systems. Earth Planet. Sci. Lett. 299, 310–316. doi:10.1016/J.EPSL.2010.09.011

Bau, M., Dulski, P., 1999. Comparing yttrium and rare earths in hydrothermal fluids from the Mid-Atlantic Ridge: implications for Y and REE behaviour during near-vent mixing and for the Y/Ho ratio of Proterozoic seawater. Chem. Geol. 155, 77–90. doi:10.1016/S0009-2541(98)00142-9

Bau, M., Dulski, P., 1995. Comparative study of yttrium and rare-earth element behaviours in fluorine-rich hydrothermal fluids. Contrib. to Mineral. Petrol. 119, 213–223. doi:10.1007/BF00307282

Bau, M., Dulski, P., Möller, P., 1995. Yttrium and holmium in South Pacific seawater: Vertical distribution and possible fractionation mechanisms. Chemie der Erde 55, 1–15.

Bau, M., Möller, P., 1992. Rare earth element fractionation in metamorphogenic hydrothermal calcite, magnesite and siderite. Mineral. Petrol. 45, 231–246. doi:10.1007/BF01163114

Bau, M., Romer, R.L., Lüders, V., Beukes, N.J., 1999. Pb, O, and C isotopes in silicified Mooidraai dolomite (Transvaal Supergroup, South Africa): implications for the composition of Paleoproterozoic seawater and ‘dating’ the increase of oxygen in the Precambrian atmosphere.

Earth Planet. Sci. Lett. 174, 43–57. doi:10.1016/S0012-821X(99)00261-7

Bau, M., Romer, R.L., Lüders, V., Dulski, P., 2003. Tracing element sources of hydrothermal mineral deposits: REE and Y distribution and Sr-Nd-Pb isotopes in fluorite from MVT deposits in the Pennine Orefield, England. Miner. Depos. 38, 992–1008. doi:10.1007/s00126-003-0376-x

Bau, M., Schmidt, K., Pack, A., Bendel, V., Kraemer, D., 2018. The European Shale: An improved data set for normalisation of rare earth element and yttrium concentrations in environmental and biological samples from Europe. Appl. Geochemistry 90, 142–149. doi:10.1016/j.apgeochem.2018.01.008

Bau, M., Usui, A., Pracejus, B., Mita, N., Kanai, Y., Irber, W., Dulski, P., 1998. Geochemistry of low-temperature water – rock interaction : evidence from natural waters, andesite, and iron-oxyhydroxide precipitates at Nishiki-numa iron-spring, Hokkaido, Japan. Chem. Geol. 151, 293–307. doi:10.1016/S0009-2541(98)00086-2

Behr, H.-J., Horn, E.E., Frentzel-Beyme, K., Reutel, C., 1987. Fluid inclusion characteristics of the Variscan and post-Variscan mineralizing fluids in the Federal Republic of Germany. Chem. Geol. 61, 273–285. doi:10.1016/0009-2541(87)90046-5

Bilal, B., Langer, P., 1987. Complex formation of trace elements in geochemical systems: stability constants of fluorocomplexes of the lanthanides in a fluorite bearing model system up to 200 °C and 1000 bar. Inorganica Chim. Acta 140, 297–298.

Boiron, M., Cathelineau, M., Richard, A., 2010. Fluid flows and metal deposition near basement ⁄ cover unconformity : lessons and analogies from Pb – Zn – F – Ba systems for the understanding of Proterozoic U deposits. Geofluids 270–292. doi:10.1111/j.1468-8123.2010.00289.x

Bolhar, R., Kamber, B.S., Moorbath, S., Fedo, C.M., Whitehouse, M.J., 2004. Characterisation of early Archaean chemical sediments by trace element signatures. Earth Planet. Sci. Lett. 222, 43–60. doi:10.1016/J.EPSL.2004.02.016

Bott, M.H.P., Smith, F.W., 2017. The role of the Devonian Weardale Granite in the emplacement of the North Pennine mineralization. Proc. Yorksh. Geol. Soc. 62, 1–15.

Bouch, J.E., Naden, J., Shepherd, T.J., McKervey, J.A., Young, B., Benham, A.J., Sloane, H.J., 2006. Direct evidence of fluid mixing in the formation of stratabound Pb–Zn–Ba–F mineralisation in the Alston Block, North Pennine Orefield (England). Miner. Depos. 41, 821–835. doi:10.1007/s00126-006-0093-3

Bouch, J.E., Naden, J., Shepherd, T.J., Young, B., Benham, A.J., Mckervey, J.A., Sloane, H.J., 2008. Stratabound Pb–Zn–Ba–F mineralisation in the Alston Block of the North Pennine Orefield (England) — origins and emplacement. British Geological Survey Research Report, RR/08/06.

Burisch, M., Marks, M.A.W., Nowak, M., Markl, G., 2016. The effect of temperature and cataclastic deformation on the composition of upper crustal fluids — An experimental approach. Chem. Geol. 433, 24–35. doi:10.1016/J.CHEMGEO.2016.03.031

Cann, J.R., Banks, D.A., 2001. Constraints on the genesis of the mineralization of the Alston Block, Northern Pennine Orefield, northern England. Proc. Yorksh. Geol. Soc. 53, 187–196. doi:10.1144/pygs.53.3.187

Castorina, F., Masi, U., Padalino, G., Palomba, M., 2008. Trace-element and Sr–Nd isotopic evidence for the origin of the Sardinian fluorite mineralization (Italy). Appl. Geochemistry 23, 2906–2921. doi:10.1016/J.APGEOCHEM.2008.04.005

Colman, T.B., Ford, T.D., Laffoley, N. d'A., 1989. 3. Metallogeny of Pennine Orefields, in: Metallogenic Models and Exploration Criteria for Buried Carbonate-Hosted Ore Deposits - a Multidisciplinary Study in Eastern England. pp. 13–23.

Crowley, S.F., Bottrell, S.H., McCarthy, M.D.B., Ward, J., Young, B., 1997. 34S of Lower Carboniferous anhydrite, Cumbria and its implications for barite mineralization in the northern Pennines. J. Geol. Soc. London. 154, 597–600. doi:10.1144/gsjgs.154.4.0597

Davison, J.M., Ineson, P.R., Mitchell, J.G., 1992. Potassium-argon isotopic age determinations from the metasomatic alteration of the Great Limestone, Northern Pennine Orefield. Proc. Yorksh. Geol. Soc. 49, 71–74. doi:10.1144/pygs.49.1.71

Dill, H.G., Hansen, B.T., Weber, B., 2011. REE contents, REE minerals and Sm/Nd isotopes of granite-

and unconformity-related fluorite mineralization at the western edge of the Bohemian Massif: With special reference to the Nabburg-Wölsendorf District, SE Germany. Ore Geol. Rev. 40, 132–148. doi:10.1016/j.oregeorev.2011.06.003

Dulski, P., 2001. Reference Materials for Geochemical Studies: New Analytical Data by ICP-MS and Critical Discussion of Reference Values. Geostand. Geoanalytical Res. 25, 87–125. doi:10.1111/j.1751-908X.2001.tb00790.x

Dunham, K.C., 1990. Geology of the Northern Pennine Orefield: I Tyne to Stainmore., in: Geological Survey of Great Britain (Ed.), Economic Memoir of the British Geological Survey, England and Wales. Stationery Office Books.

Dunham, K.C., Fitch, F.J., Ineson, P.R., Miller, J.A., Mitchell, J.G., 1968. The Geochronological Significance of Argon-40/Argon-39 Age Determinations on White Whin from the Northern Pennine Orefield. Proc. R. Soc. Lond. A. Math. Phys. Sci. doi:10.2307/2416205

Dunham, K.C., Wilson, A.A., 1985. Geology of the Northern Pennine Orefield: 2 Stainmore to Craven, in: Geological Survey of Great Britain (Ed.), Economic Memoir of the British Geological Survey, England and Wales. Stationery Office Books.

Dunham, S.K., 1974. Granite beneath the Pennines in Northern Yorkshire. Proc. Yorksh. Geol. Soc. 40, 191–194. doi:10.1144/pygs.40.2.191

Evans, D.J., Walker, A.S.D., Chadwick, R.A., 2002. The Pennine Anticline, northern England - a continuing enigma? Proc. Yorksh. Geol. Soc. 54, 17–34. doi:10.1144/pygs.54.1.17

Ewbank, G., Manning, D.A.C., Abbott, G.D., 1995. The relationship between bitumens and mineralization in the South Pennine Orefield, central England. J. Geol. Soc. London. 152, 751–765. doi:10.1144/gsjgs.152.5.0751

Fisher, J., Lillie, R., Rakovan, J., 2013. Fluorite in mississippi valley-type deposits. Rocks Miner. 88, 20–47. doi:10.1080/00357529.2013.747895

Fitch, F.J., Miller, J.A., 1967. The age of the Whin Sill. Geol. J. 5, 233–250.

Fontes, J.C., Matray, J.M., 1993. Geochemistry and origin of formation brines from the Paris Basin,

France: 1. Brines associated with Triassic salts. Chem. Geol. 109, 149–175. doi:10.1016/0009-2541(93)90068-T

Ford, T.D., Worley, N.E., 2016. Mineralization of the South Pennine Orefield, UK—A Review. Proc. Yorksh. Geol. Soc. 61, 55–86. doi:10.1144/pygs2015-364

Galindo, C., Tornos, F., Darbyshire, D.P.F., Casquet, C., 1994. The age and origin of the barite-fluorite (Pb□Zn) veins of the Sierra del Guadarrama (Spanish Central System, Spain): a radiogenic (Nd, Sr) and stable isotope study. Chem. Geol. 112, 351–364. doi:10.1016/0009-2541(94)90034-5

Giese, U., Bau, M., 1994. Trace element accessibility in mid-ocean ridge and ocean island basalt: an experimental approach. Mineral. Mag. 58A, 329–330.

Göb, S., Loges, A., Nolde, N., Bau, M., Jacob, D.E., Markl, G., 2013. Major and trace element compositions (including REE) of mineral, thermal, mine and surface waters in SW Germany and implications for water–rock interaction. Appl. Geochemistry 33, 127–152. doi:10.1016/J.APGEOCHEM.2013.02.006

Govindaraju, K., Potts, P.J., Webb, P.C., Watson, J.S., 1994. 1994 Report on Whin Sill Dolerite WS-E from England and Pitscurrie microgabbro PM-S from Scotland: Assessment by one hundred and four international laboratories. Geostand. Geoanalytical Res. 18, 211–300. doi:10.1111/j.1751-908X.1994.tb00520.x

Grandia, F., Cardellach, E., Canals, A., Banks, D.A., 2003. Geochemistry of the Fluids Related to Epigenetic Carbonate-Hosted Zn-Pb Deposits in the Maestrat Basin, Eastern Spain: Fluid Inclusion and Isotope (Cl, C, O, S, Sr) Evidence. Econ. Geol. 98, 933–954. doi:10.2113/gsecongeo.98.5.933

Graupner, T., Mühlbach, C., Schwarz-Schampera, U., Henjes-Kunst, F., Melcher, F., Terblanche, H., 2015. Mineralogy of high-field-strength elements (Y, Nb, REE) in the world-class Vergenoeg fluorite deposit, South Africa. Ore Geol. Rev. 64, 583–601. doi:10.1016/j.oregeorev.2014.02.012

Heijlen, W., Muchez, P., Banks, D.A., 2001. Origin and evolution of high-salinity, Zn-Pb mineralising fluids in the Variscides of Belgium. Miner. Depos. 36, 165–176. doi:10.1007/s001260050296

Heijlen, W., Muchez, P., Banks, D.A., Schneider, J., Kucha, H., Keppens, E., 2003. Carbonate-Hosted Zn-Pb Deposits in Upper Silesia, Poland: Origin and Evolution of Mineralizing Fluids and Constraints on Genetic Models. Econ. Geol. 98, 911–932. doi:10.2113/gsecongeo.98.5.911

Herut, B., Starinsky, A., Katz, A., Bein, A., 1990. The role of seawater freezing in the formation of subsurface brines. Geochim. Cosmochim. Acta 54, 13–21. doi:10.1016/0016-7037(90)90190-V

Holland, J.G., Lambert, R., 1970. Weardale Granite. Trans. Nat. Hist. Soc. Northumberland, Durham Newcastle- upon-Tyne 41, 103–118.

Ineson, P.R., 1976. Ores of the northern Pennines, the Lake District and North Wales, in: Wolf, K.H. (Ed.), Handbook of Stratabound and Stratiform Ore Deposits. Elsevier, pp. 197–230.

Jones, D.G., Swainbank, I.G., 1993. Leachate lead isotope studies of potential sources of the South Pennine Orefield of England, in: Current Research in Geology Applied to Ore Deposits. Proceedings 2nd Biennial SGA Meeting, Granada. pp. 139–142.

Kraemer, D., Kopf, S., Bau, M., 2015. Oxidative mobilization of cerium and uranium and enhanced release of “immobile” high field strength elements from igneous rocks in the presence of the biogenic siderophore desferrioxamine B. Geochim. Cosmochim. Acta 165, 263–279. doi:10.1016/j.gca.2015.05.046

Kullerud, K., 1996. Chlorine-rich amphiboles: interplay between amphibole composition and an evolving fluid. Eur. J. Mineral. 8, 355–370. doi:10.1127/ejm/8/2/0355

Leach, D.L., Bradley, D., Lewchuk, M.T., Symons, D.T., de Marsily, G., Brannon, J., 2001. Mississippi Valley-type lead–zinc deposits through geological time: implications from recent age-dating research. Miner. Depos. 36, 711–740. doi:10.1007/s001260100208

Lee Davisson, M., Criss, R.E., 1996. Na□Ca□Cl relations in basinal fluids. Geochim. Cosmochim. Acta 60, 2743–2752. doi:10.1016/0016-7037(96)00143-3

Loges, A., Wagner, T., Barth, M., Bau, M., Göb, S., Markl, G., 2012. Negative Ce anomalies in Mn oxides: The role of Ce4+ mobility during water–mineral interaction. Geochim. Cosmochim. Acta 86, 296–317. doi:10.1016/j.gca.2012.03.017

Lüders, V., Möller, P., 1992. Fluid evolution and ore deposition in the Harz Mountains (Germany). Eur. J. Mineral. 4, 1053–1068. doi:10.1127/ejm/4/5/1053

Markl, G., Bucher, K., 1998. Composition of fluids in the lower crust inferred from metamorphic salt in lower crustal rocks. Nature 391, 781–783. doi:10.1038/35836

McCaig, A.., Tritlla, J., Banks, D.., 2000. Fluid mixing and recycling during Pyrenean thrusting: evidence from fluid inclusion halogen ratios. Geochim. Cosmochim. Acta 64, 3395–3412. doi:10.1016/S0016-7037(00)00437-3

Migdisov, A.A., Williams-Jones, A.E., 2014. Hydrothermal transport and deposition of the rare earth elements by fluorine-bearing aqueous liquids. Miner. Depos. 49, 987–997. doi:10.1007/s00126-014-0554-z

Möller, P., 1998. Europium anomalies in hydrothermal minerals. Kinetic versus thermodynamic interpretation, in: Proceedings of the Ninth Quadrennial IAGOD Symposium. pp. 239–246.

Möller, P., Maus, H., Gundlach, H., 1982. Die Entwicklung von Flußspatmineralisationen im Bereich des Schwarzwaldes, in: Jahresh. Geol. Landesamtes Baden-Württ. pp. 35–70.

Muchez, P., Heijlen, W., Banks, D., Boni, M., Grandia, F., 2005. 7: Extensional tectonics and the timing and formation of basin-hosted deposits in Europe. Ore Geol. Rev. 27, 241–267. doi:10.1016/J.OREGEOREV.2005.07.013

Munoz, M., Boyce, A.J., Courjault-Radé, P., Fallick, A.E., Tollon, F., 1999. Continental basinal origin of ore fluids from southwestern Massif central fluorite veins (Albigeois, France): evidence from fluid inclusion and stable isotope analyses. Appl. Geochemistry 14, 447–458. doi:10.1016/S0883-2927(98)00070-5

Munoz, M., Boyce, A.J., Courjault-Radé, P., Fallick, A.E., Tollon, F., 1994. Multi-stage fluid incursion in the Palaeozoic basement-hosted Saint-Salvy ore deposit (NW Montagne Noire, southern France). Appl. Geochemistry 9, 609–626. doi:10.1016/0883-2927(94)90022-1

Munoz, M., Premo, W.R., Courjault-Radé, P., 2005. Sm-Nd dating of fluorite from the worldclass Montroc fluorite deposit, southern Massif Central, France. Miner. Depos. 39, 970–975.

doi:10.1007/s00126-004-0453-9

Piqué, À., Canals, À., Grandia, F., Banks, D.A., 2008. Mesozoic fluorite veins in NE Spain record regional base metal-rich brine circulation through basin and basement during extensional events. Chem. Geol. 257, 139–152. doi:10.1016/J.CHEMGEO.2008.08.028

Plant, J.A., Jones, D.G., Brown, G.C., Colman, T.B., Cornwell, J.D., Smith, K., Smith, N.J.P., Walker, A.S.D., Webb, P.C., 1988. Metallogenic models and exploration criteria for buried carbonate-hosted ore deposits: Results of a multidisciplinary study in eastern England, in: Boissonnas, J., Omenetto, P. (Eds.), Mineral Deposits within the European Community. Springer Verlag, Berlin, pp. 321–352.

Plumlee, G.S., Goldhaber, M.B., Rowan, E.L., 1995. The potential role of magmatic gases in the genesis of Illinois-Kentucky fluorspar deposits; implications from chemical reaction path modeling. Econ. Geol. 90, 999–1011. doi:10.2113/gsecongeo.90.5.999

Rajabzadeh, M.A., 2007. A Fluid Inclusion Study of a Large MVT Barite-Fluorite Deposit: Komshecheh, Iran. Springer 31, 73–87. doi:10.22099/IJSTS.2007.2318

Rankin, A.H., Graham, M.J., 1988. Na, K and Li contents of mineralizing fluids in the Northern Pennine Orefield, England, and their genetic significance. Trans. Inst. Min. Metall. London 97, B99–B107.

Rogers, P.J., 1978. Fluid Inclusion Studies on Fluorite from Askrigg Block. Trans. Inst. Min. Met. 88.

Sánchez, V., Cardellach, E., Corbella, M., Vindel, E., Martín-Crespo, T., Boyce, A.J., 2010. Variability in fluid sources in the fluorite deposits from Asturias (N Spain): Further evidences from REE, radiogenic (Sr, Sm, Nd) and stable (S, C, O) isotope data. Ore Geol. Rev. 37, 87–100. doi:10.1016/J.OREGEOREV.2009.12.001

Sawkins, F.J., 1966. Ore genesis in the North Pennine Orefield, in the light of fluid inclusion studies. Econ. Geol. 61, 385–401.

Schier, K., Bau, M., Münker, C., Beukes, N., Viehmann, S., 2018. Trace element and Nd isotope composition of shallow seawater prior to the Great Oxidation Event: Evidence from stromatolitic bioherms in the Paleoproterozoic Rooinekke and Nelani Formations, South Africa.

Precambrian Res. 315, 92–102. doi:10.1016/J.PRECAMRES.2018.07.014

Schmidt, K., Garbe-Schönberg, D., Bau, M., Koschinsky, A., 2010. Rare earth element distribution in >400 °C hot hydrothermal fluids from 5°S, MAR: The role of anhydrite in controlling highly variable distribution patterns. Geochim. Cosmochim. Acta 74, 4058–4077. doi:10.1016/J.GCA.2010.04.007

Schwinn, G., Markl, G., 2005. REE systematics in hydrothermal fluorite. Chem. Geol. 216, 225–248. doi:10.1016/J.CHEMGEO.2004.11.012

Shepherd, T.J., Darbyshire, D.P.F., Moore, G.R., 1982. Rare earth element and isotopic geochemistry of the North Pennine ore deposits. Bull Bur Mech Gites Min 11, 371–377.

Shibata, S., Tanaka, T., Yamamoto, K., 2006. Crystal structure control of the dissolution of rare earth elements in water-mineral interactions. Geochem. J. 40, 437–446. doi:10.2343/geochemj.40.437

Sizaret, S., Marcoux, E., Jebrak, M., Touray, J.C., 2004. The Rossignol Fluorite Vein, Chaillac, France: Multiphase Hydrothermal Activity and Intravein Sedimentation. Econ. Geol. 99, 1107–1122. doi:10.2113/gsecongeo.99.6.1107

Small, A.T., 1977. Mineralization of the stainmore depression and northern part of the askrigg block - Durham theses. Durham University.

Solomon, M., 1966. Origin of barite in the North Pennine orefield. Trans. Inst. Min. Metall. London B75, 230–231.

Solomon, M., Rafter, T.A., Dunham, K.C., 1971. Sulphur and oxygen isotope studies in the northern Pennines in relation to ore genesis. Trans. Inst. Min. Metall. London, B80, 259–275.

Souissi, F., Souissi, R., Dandurand, J.-L., 2010. The Mississippi Valley-type fluorite ore at Jebel Stah (Zaghouan district, north-eastern Tunisia): Contribution of REE and Sr isotope geochemistries to the genetic model. Ore Geol. Rev. 37, 15–30. doi:10.1016/J.OREGEOREV.2009.11.001

Staude, S., Bons, P.D., Markl, G., 2009. Hydrothermal vein formation by extension-driven dewatering of the middle crust: An example from SW Germany. Earth Planet. Sci. Lett. 286, 387–395.

doi:10.1016/J.EPSL.2009.07.012

Stober, I., Bucher, K., 1999. Origin of salinity of deep groundwater in crystalline rocks. Terra Nov. 11, 181–185. doi:10.1046/j.1365-3121.1999.00241.x

Stone, P, Millward, D, Young, B, Merritt, J W, Clarke, S M, McCormac, M and Lawrence, D.J.D., 2010. British regional geology: Northern England, Fifth. ed. British Geological Survey, NERC, Keyworth, Nottingham.

Subías, I., Fernández-Nieto, C., 1995. Hydrothermal events in the Valle de Tena (Spanish Western Pyrenees) as evidenced by fluid inclusions and trace-element distribution from fluorite deposits. Chem. Geol. 124, 267–282. doi:10.1016/0009-2541(95)00060-Y

Subías, I., Moritz, R., Fernández-Nieto, C., 1998. Isotopic composition of strontium in the Valle de Tena (Spanish Central Pyrenees) fluorite deposits: relevance for the source of elements and genetic significance. Miner. Depos. 33, 416–424. doi:10.1007/s001260050159

Sverjensky, D.A., 1984. Europium redox equilibria in aqueous solution. Earth Planet. Sci. Lett. 67, 70–78.

Tornos, F., Delgado, A., Casquet, C., Galindo, C., 2000. 300 Million years of episodic hydrothermal activity: stable isotope evidence from hydrothermal rocks of the Eastern Iberian Central System. Miner. Depos. 35, 551–569. doi:10.1007/s001260050261

Ulrich, M.R., Bodnar, R.J., 1988. Systematics of stretching of fluid inclusions; II, Barite at 1 atm confining pressure. Econ. Geol. 83, 1037–1046. doi:10.2113/gsecongeo.83.5.1037

Vaughan, D.J., Ixer, R.A., 1980. Studies of sulphide mineralogy of north Pennine ores and its contribution to genetic models. Trans. Inst. Min. Metall. London 89, B99–B110.

Walter, B.F., Burisch, M., Markl, G., 2016. Long-term chemical evolution and modification of continental basement brines - a field study from the Schwarzwald, SW Germany. Geofluids 16, 604–623. doi:10.1111/gfl.12167

Webb, P.C., Brown, G.C., 1989. Geochemistry of pre-mesozoic igneous rocks, in: Plant, J.A., Jones, D.G. (Eds.), Metallogenic Models and Exploration Criteria for Buried Carbonate-Hosted Ore

Deposits - a Multidisciplinary Study in Eastern England. Springer Science+Business Media, pp. 95–121.

Wegner, W., Koeberl, C., 2016. Strontium and neodymium isotope systematics of target rocks and impactites from the El'gygytgyn impact structure: Linking impactites and target rocks. Meteorit. Planet. Sci. 51, 2347–2365. doi:10.1111/maps.12731

Williams-Jones, A.E., Migdisov, A.A., Samson, I.M., 2012. Hydrothermal Mobilisation of the Rare Earth Elements - a Tale of "Ceria" and "Yttria." Elements 8, 355–360. doi:10.2113/gselements.8.5.355

8. Figure captions

Fig. 1: Sketch map showing the extent of the Northern Pennine Orefield (NPO) and the Southern Pennine Orefield (SPO) in Great Britain as well as simplified geological map of the NPO showing the uplifted crustal blocks, associated faults and granitic batholiths (red). Modified after Stone et al. (2010).

Fig. 2a-b: Na/Br vs. Cl/Br molar ratios of crush leach data for fluorite, quartz, calcite, sphalerite and barite specimen from the Alston Block, northern part of the NPO, and the Askrigg Block, southern part of the NPO. The numbers correspond to the sample numbers in the data tables. Settlingstones is a barite mine to the north of the main orefield in the Northumberland Trough. The arrowed line represents the evaporation trend for evaporating seawater (data from Fontes and Matray, 1993).

Figs. 3a-c: PAAS-normalized REY (REY_{SN}) plots of fluorite samples from the Alston Block (a) and from the Askrigg Block (b) in comparison to potential source rocks (c). Note the up to two orders of magnitude difference in the concentrations of specific REY and the presence of positive Eu_{SN} anomalies in fluorites from the Alston Block and absence of or negative Eu anomalies in the Askrigg fluorites.

Fig. 4: Graph of Y vs. Ho for fluorites from the Askrigg Block (blue) and the Alston Block (red) of the Northern Pennine Orefield (this study) compared to Frazer's Hush Mine fluorites from the NPO (grey diamonds) and SPO fluorites (grey triangles) from Bau et al. (2003).

Fig. 5: Graph of Ce_{SN}/Ce^{*}_{SN} vs. Eu_{SN}/Eu^{*}_{SN} indicating potential anomalous behaviour of redox-sensitive REY Ce and Eu in fluorites from the NPO. Note the pronounced positive Eu_{SN} anomalies in

Alston Block fluorites, the negative Ce_{SN} anomalies in Askrigg Block fluorites and the close similarity of Askrigg Block fluorites to SPO fluorites from Bau et al. (2003).

Fig. 6: $^{87}Sr/^{86}Sr$ against $^{143}Nd/^{144}Nd$ isotope ratio plot of the fluorite samples investigated in this study. The 2σ-errors are smaller than symbol size. Note that Alston and Askrigg Block fluorites plot in different clusters and their isotopic signatures differ significantly from published SPO fluorites, from the carbonate host rocks and from the Whin Sill dolerite reference material WS-E.

Fig. 7: $^{143}Nd/^{144}Nd$ plotted against the reciprocal of the Nd concentration (a) and $^{87}Sr/^{86}Sr$ against the respective reciprocal of the Sr concentration (b).

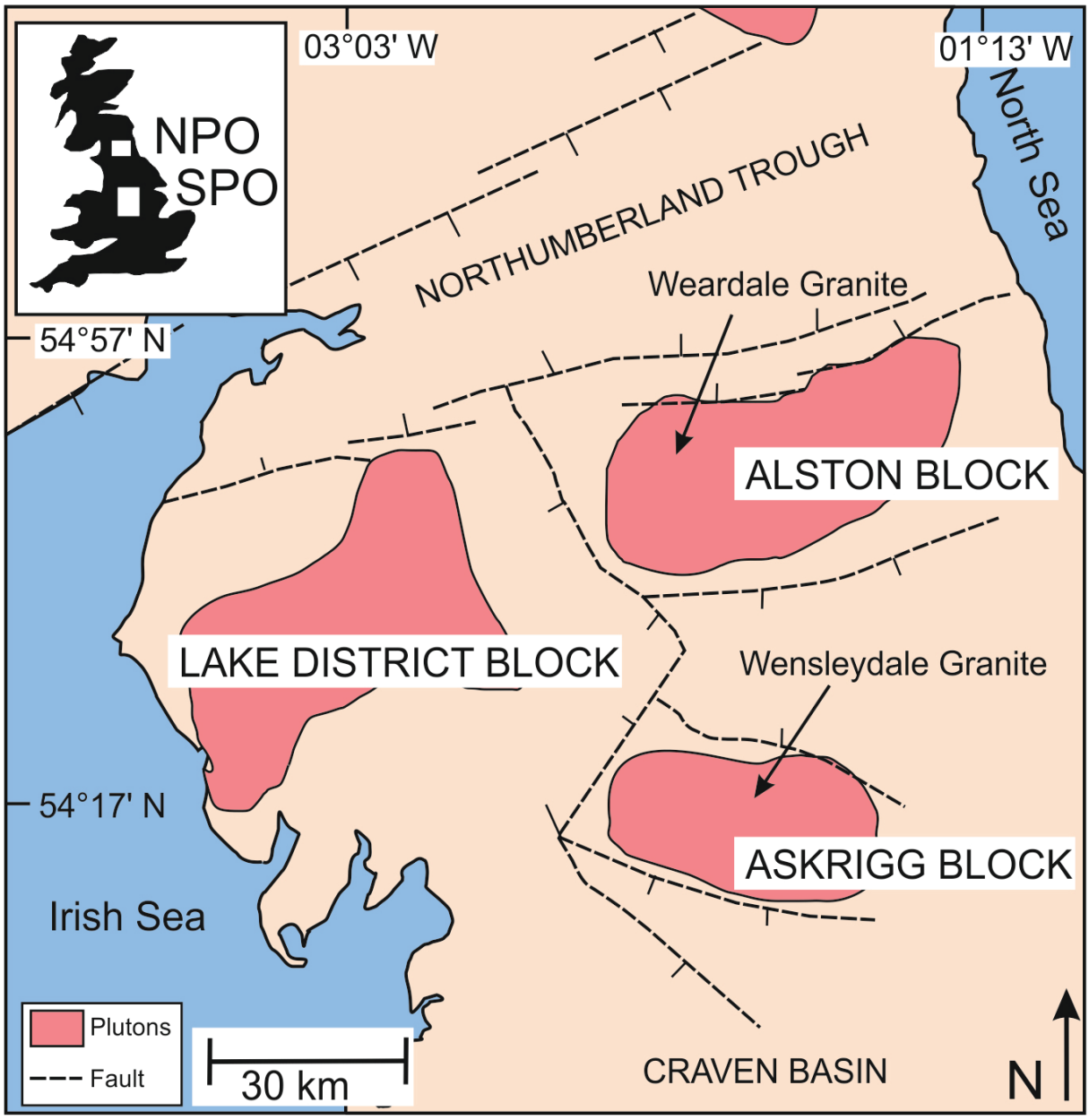
NPO
SPO
03°03' W
01°13' W
North Sea
NORTHUMBERLAND TROUGH
Weardale Granite
54°57' N
ALSTON BLOCK
LAKE DISTRICT BLOCK
Wensleydale Granite
54°17' N
ASKRIGG BLOCK
Irish Sea
Plutons
Fault
30 km
CRAVEN BASIN
N

a)

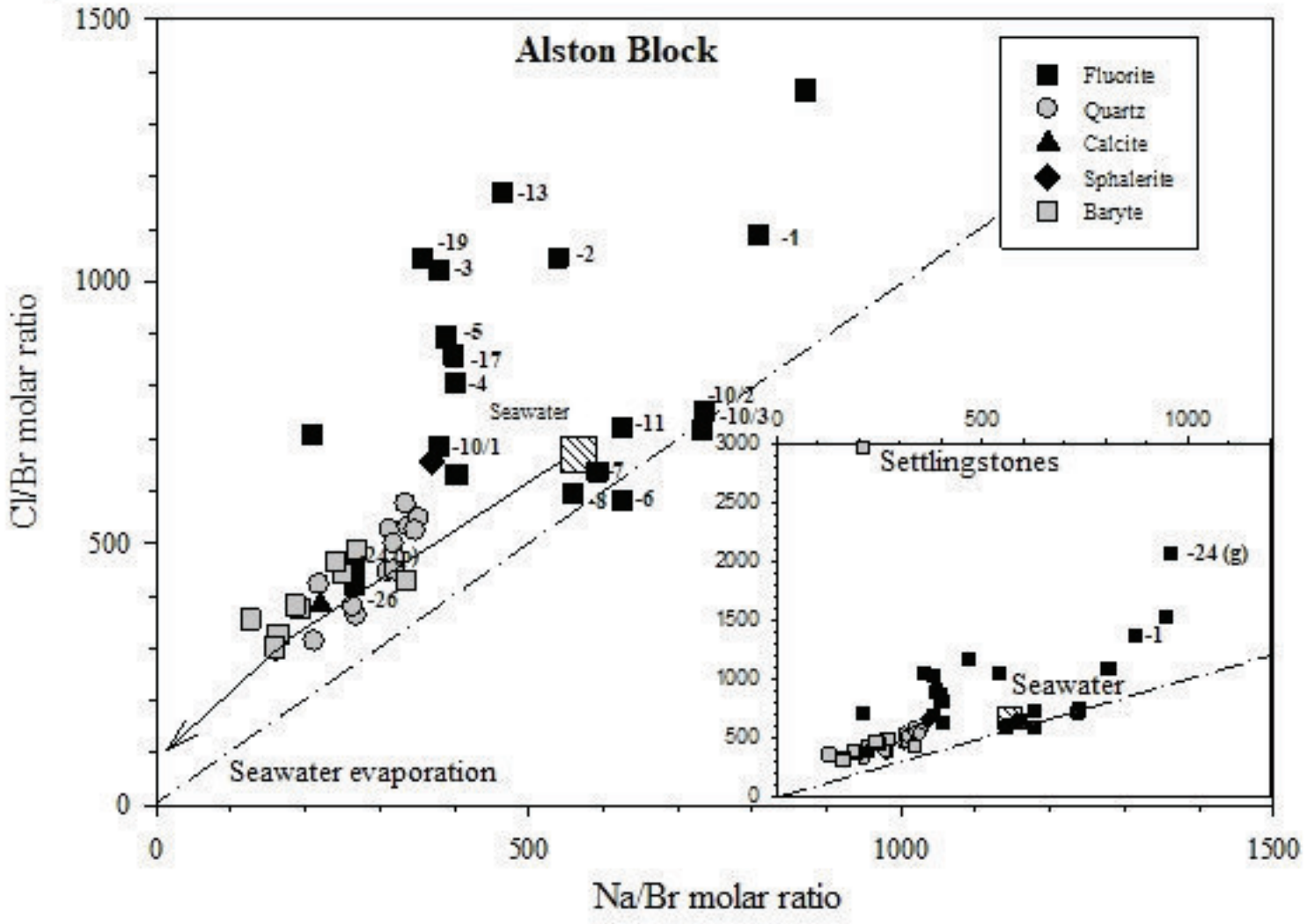
Alston Block
Fluorite
Quartz
Calcite
Sphalerite
Baryte
Cl/Br molar ratio
Na/Br molar ratio
Seawater
Seawater evaporation
-13
-19
-3
-2
-1
-5
-17
-4
-10/2
-10/3
-11
-10/1
-7
-8
-6
-26
0
500
1000
1500
Settlingstones
-24 (g)
-1
Seawater
2000
2500
3000

b)

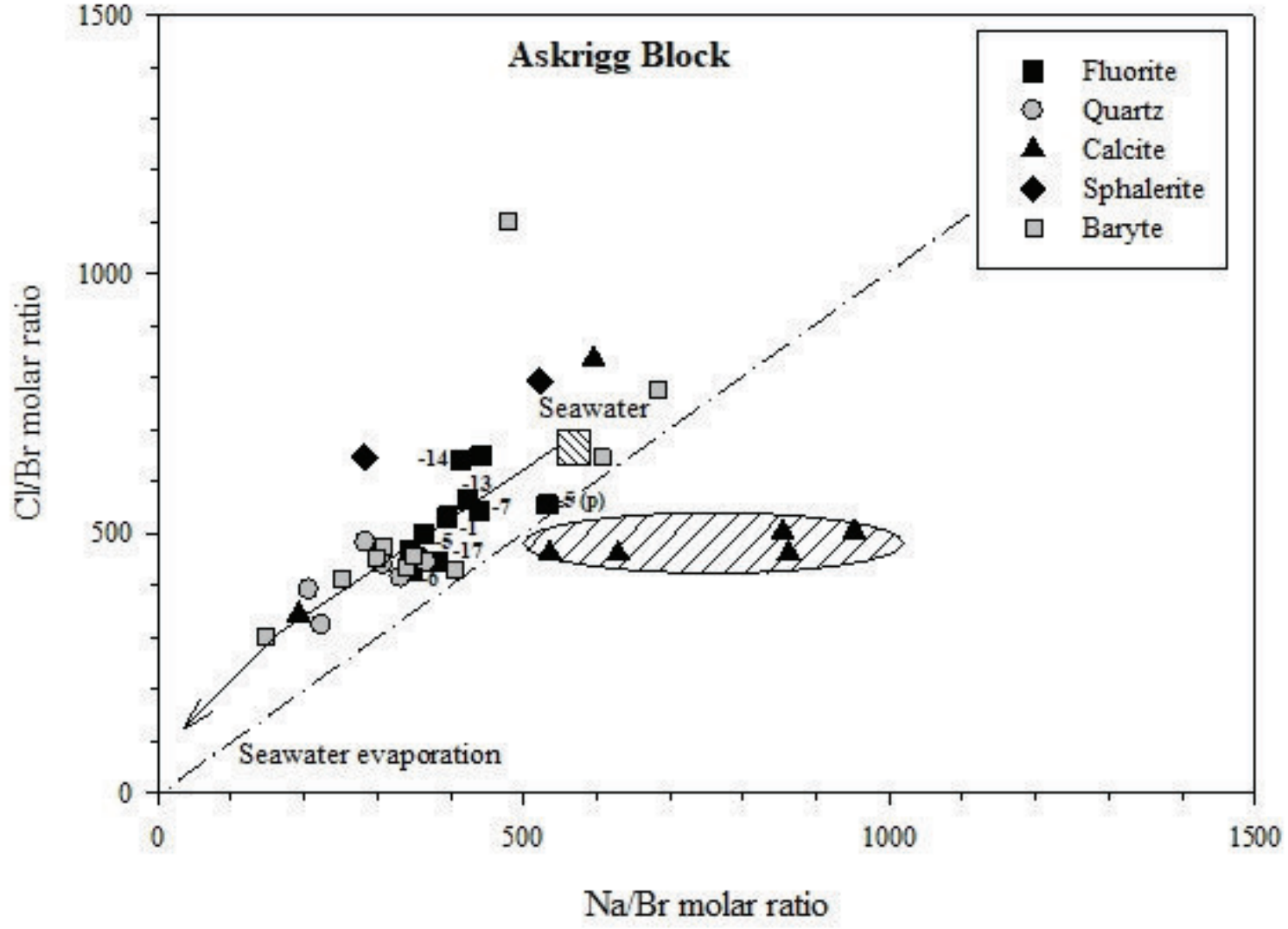
Askrigg Block
Fluorite
Quartz
Calcite
Sphalerite
Baryte
Seawater
Seawater evaporation
-14
-13
-7
-5 (p)
-1
-5
-17
-6
Cl/Br molar ratio
Na/Br molar ratio
0
500
1000
1500

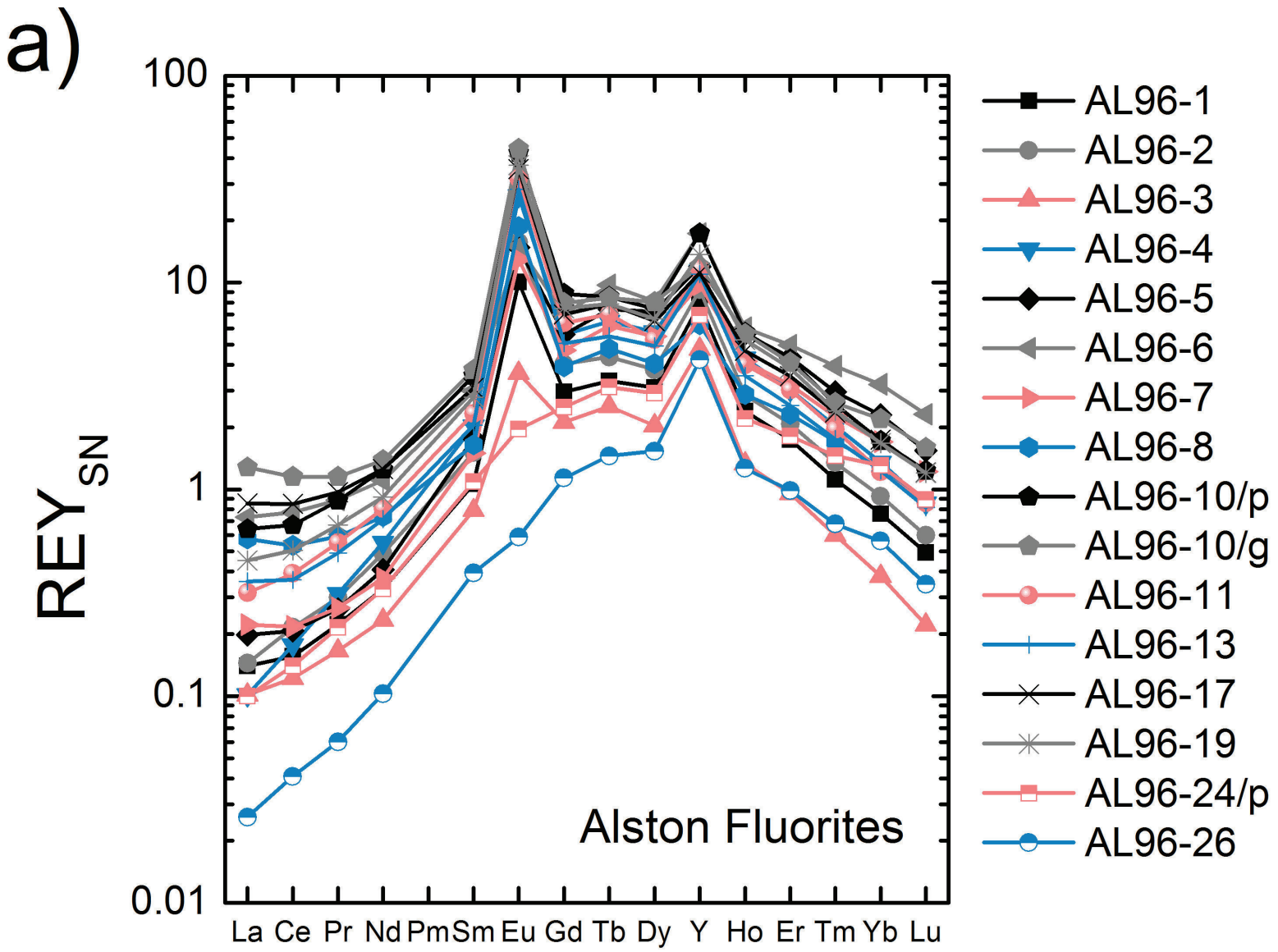
a)
100
10
1
0.1
0.01
REY SN
La Ce Pr Nd Pm Sm Eu Gd Tb Dy Y Ho Er Tm Yb Lu
Alston Fluorites
AL96-1
AL96-2
AL96-3
AL96-4
AL96-5
AL96-6
AL96-7
AL96-8
AL96-10/p
AL96-10/g
AL96-11
AL96-13
AL96-17
AL96-19
AL96-24/p
AL96-26

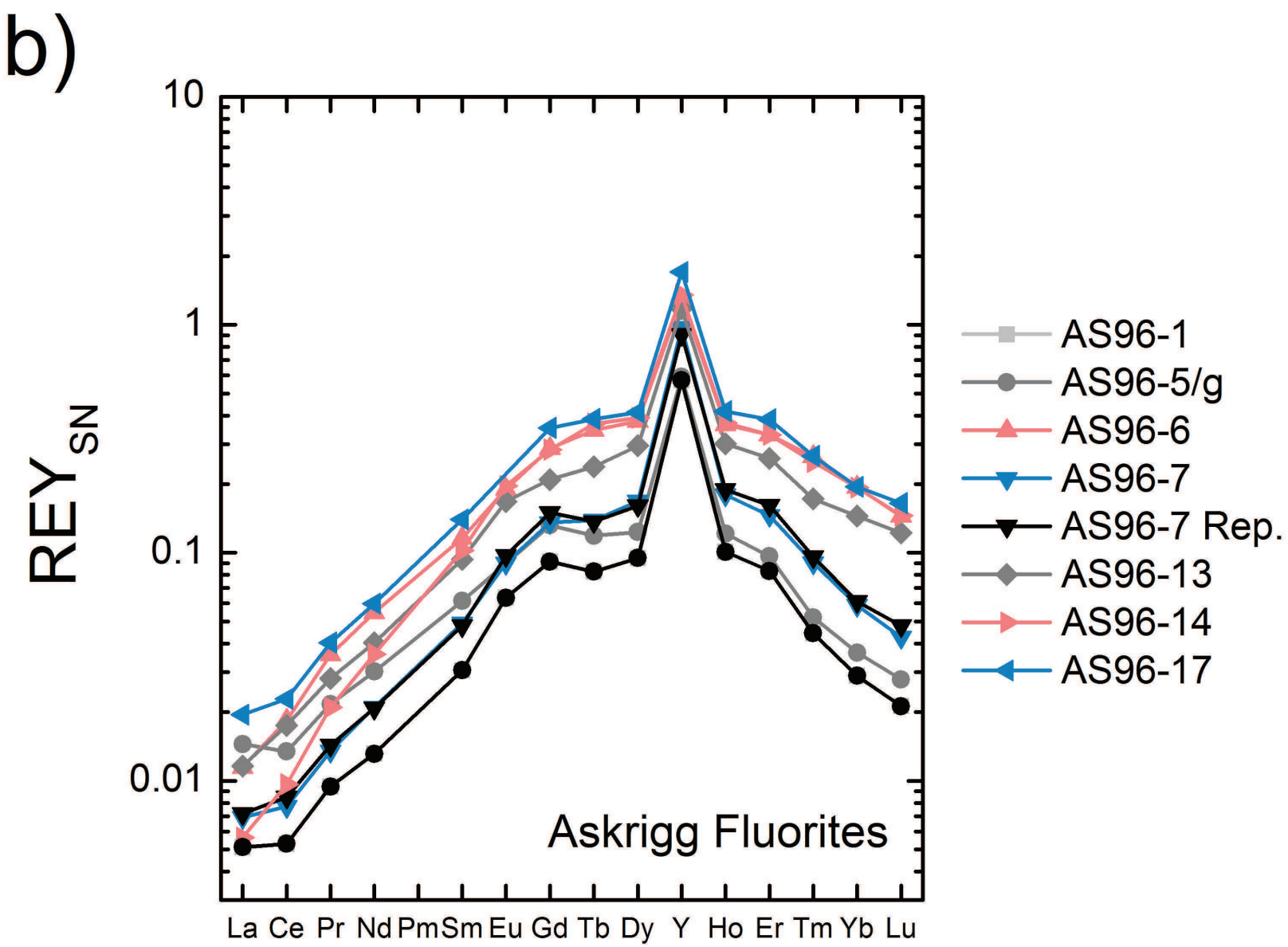
b)
10
1
0.1
0.01
REY SN
La Ce Pr Nd Pm Sm Eu Gd Tb Dy Y Ho Er Tm Yb Lu
Askrigg Fluorites
AS96-1
AS96-5/g
AS96-6
AS96-7
AS96-7 Rep.
AS96-13
AS96-14
AS96-17

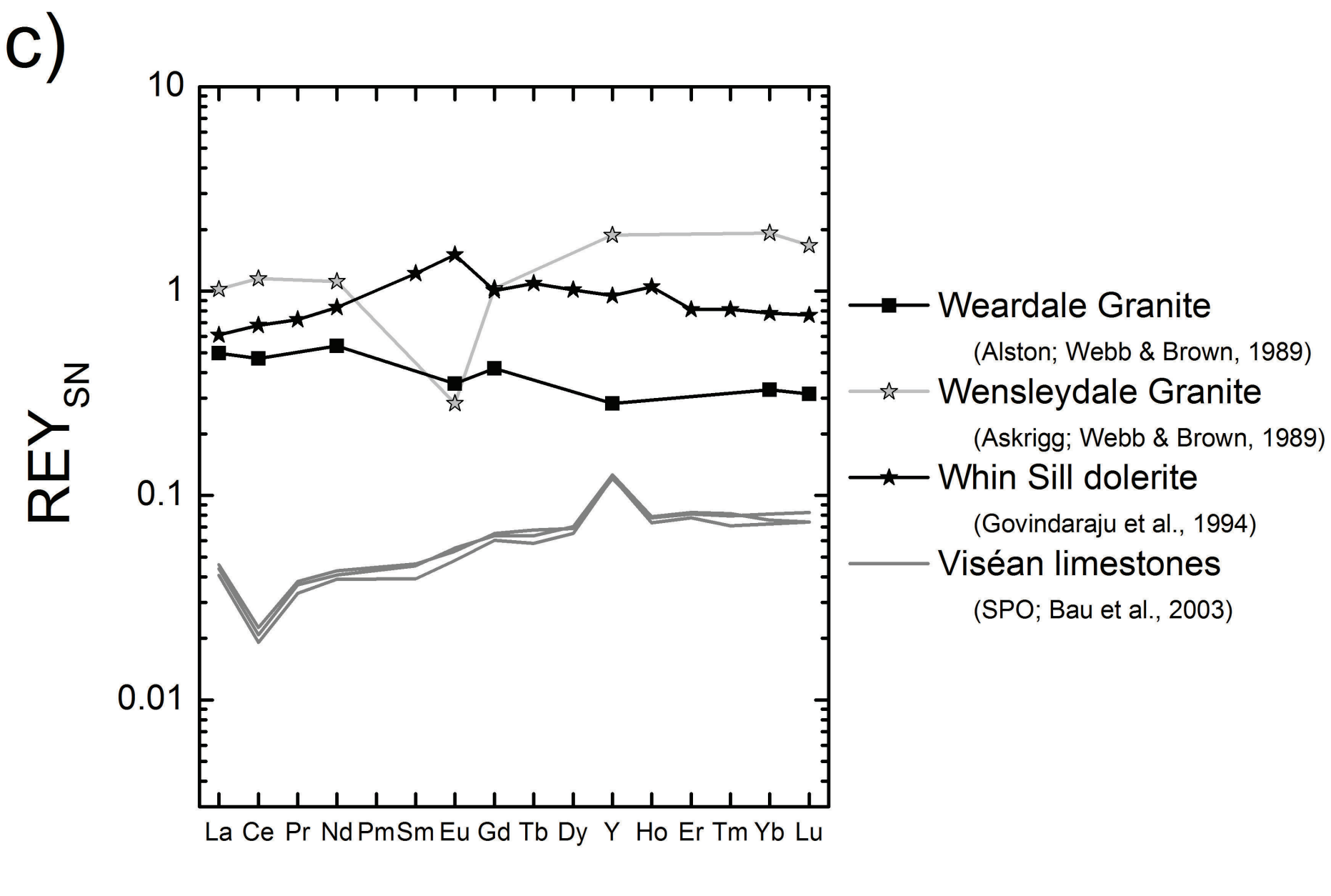
c)
10
1
0.1
0.01
REY SN
La Ce Pr Nd Pm Sm Eu Gd Tb Dy Y Ho Er Tm Yb Lu
Weardale Granite
(Alston; Webb & Brown, 1989)
Wensleydale Granite
(Askrigg; Webb & Brown, 1989)
Whin Sill dolerite
(Govindaraju et al., 1994)
Viséan limestones
(SPO; Bau et al., 2003)

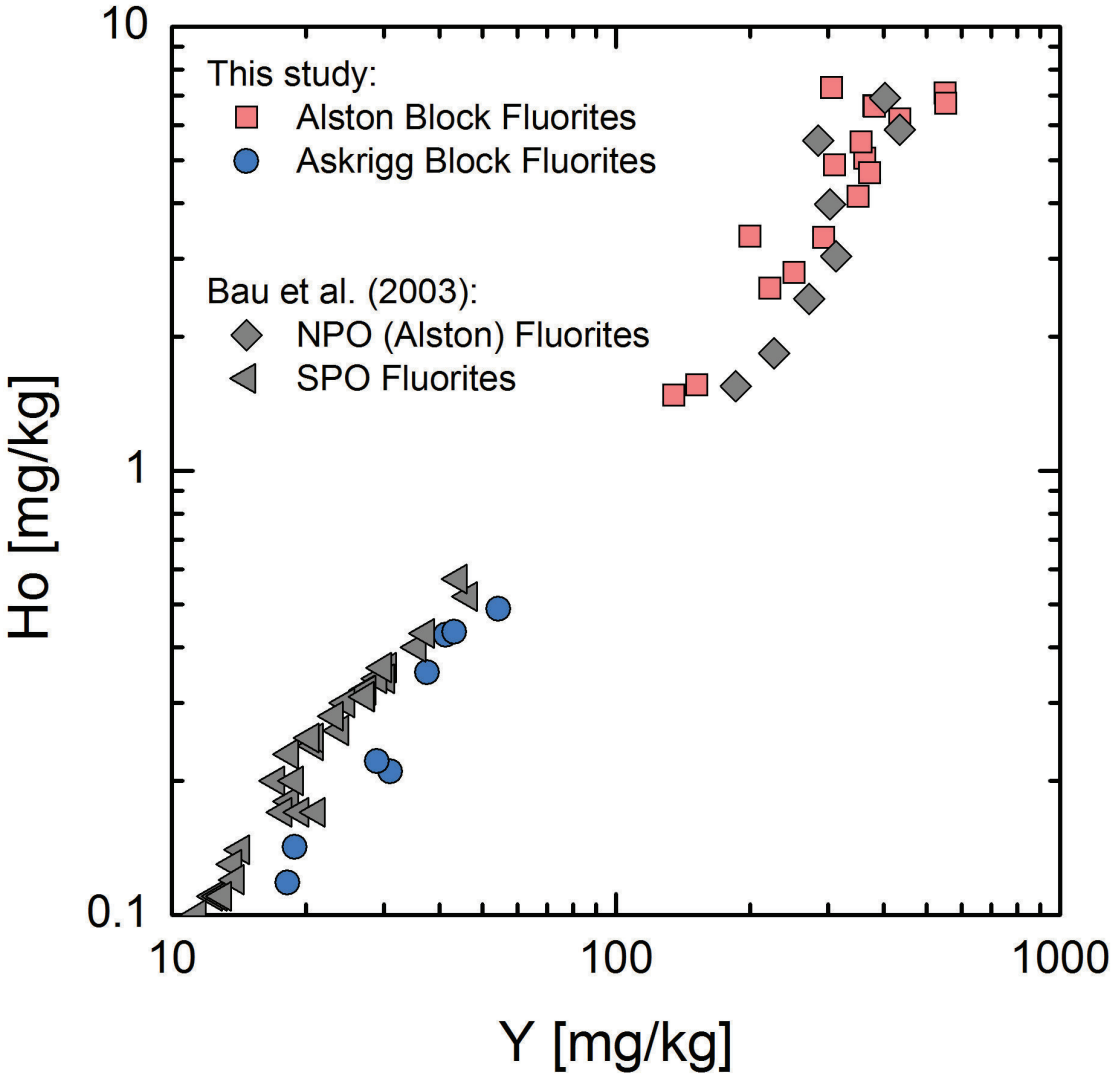
This study:
Alston Block Fluorites
Askrigg Block Fluorites
Bau et al. (2003):
NPO (Alston) Fluorites
SPO Fluorites
Ho [mg/kg]
Y [mg/kg]
10
1
0.1
10
100
1000

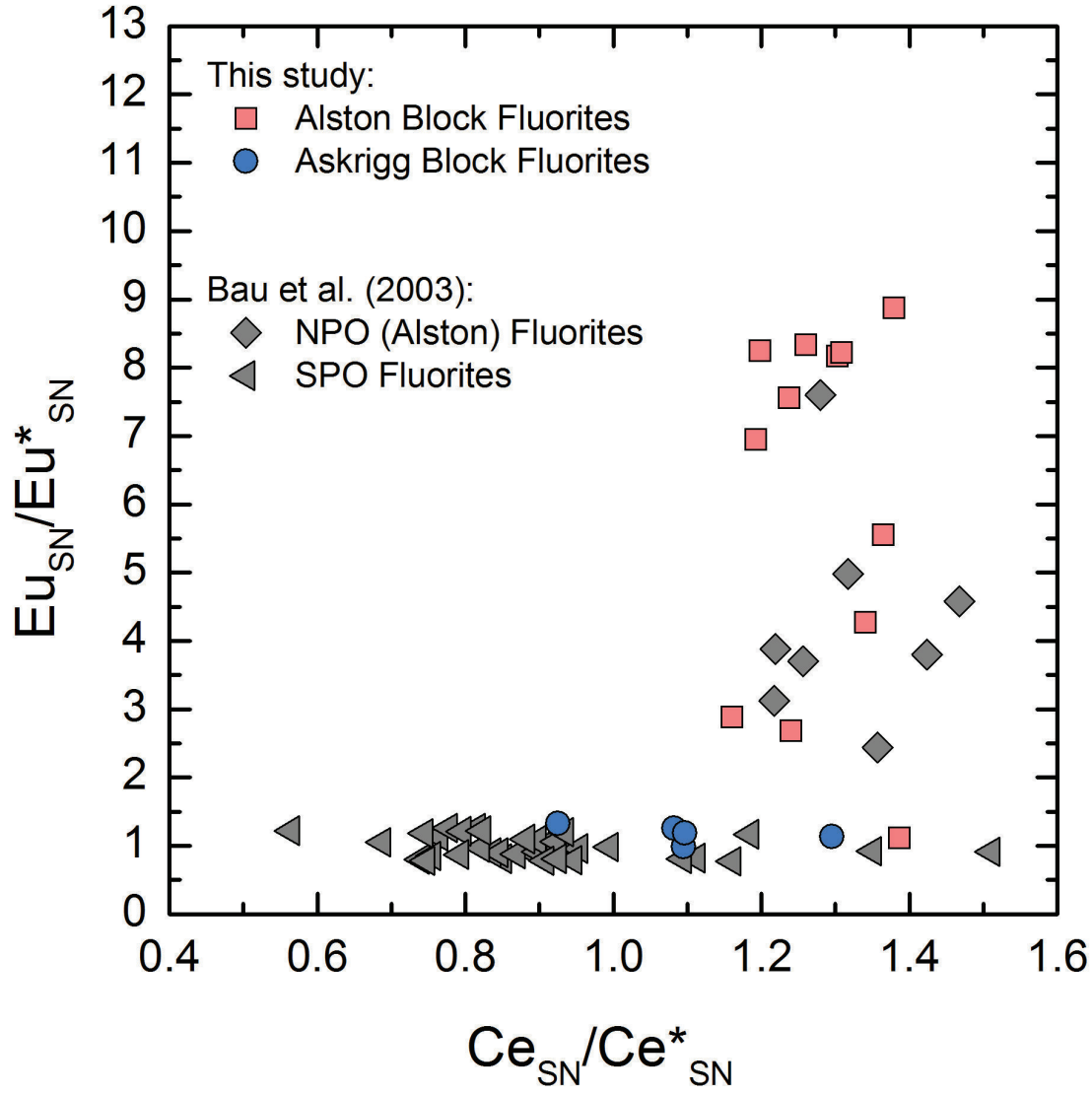
This study:
Alston Block Fluorites
Askrigg Block Fluorites
Bau et al. (2003):
NPO (Alston) Fluorites
SPO Fluorites
Eu_SN/Eu*_SN
Ce_SN/Ce*_SN
0
1
2
3
4
5
6
7
8
9
10
11
12
13
0.4
0.6
0.8
1.0
1.2
1.4
1.6

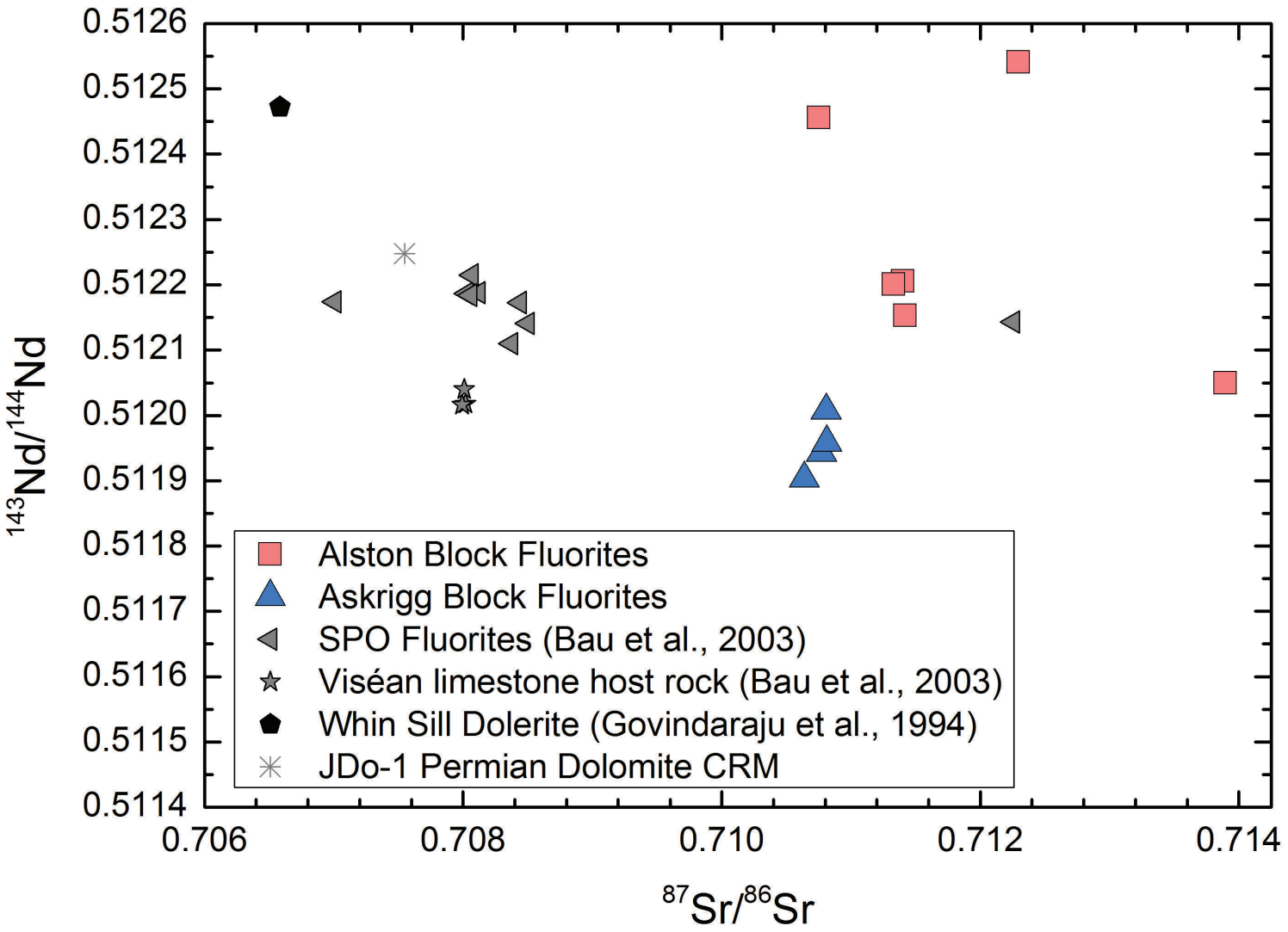
0.5126
0.5125
0.5124
0.5123
0.5122
0.5121
0.5120
0.5119
0.5118
0.5117
0.5116
0.5115
0.5114
$^{143}Nd/^{144}Nd$
0.706
0.708
0.710
0.712
0.714
$^{87}Sr/^{86}Sr$
Alston Block Fluorites
Askrigg Block Fluorites
SPO Fluorites (Bau et al., 2003)
Viséan limestone host rock (Bau et al., 2003)
Whin Sill Dolerite (Govindaraju et al., 1994)
JDo-1 Permian Dolomite CRM

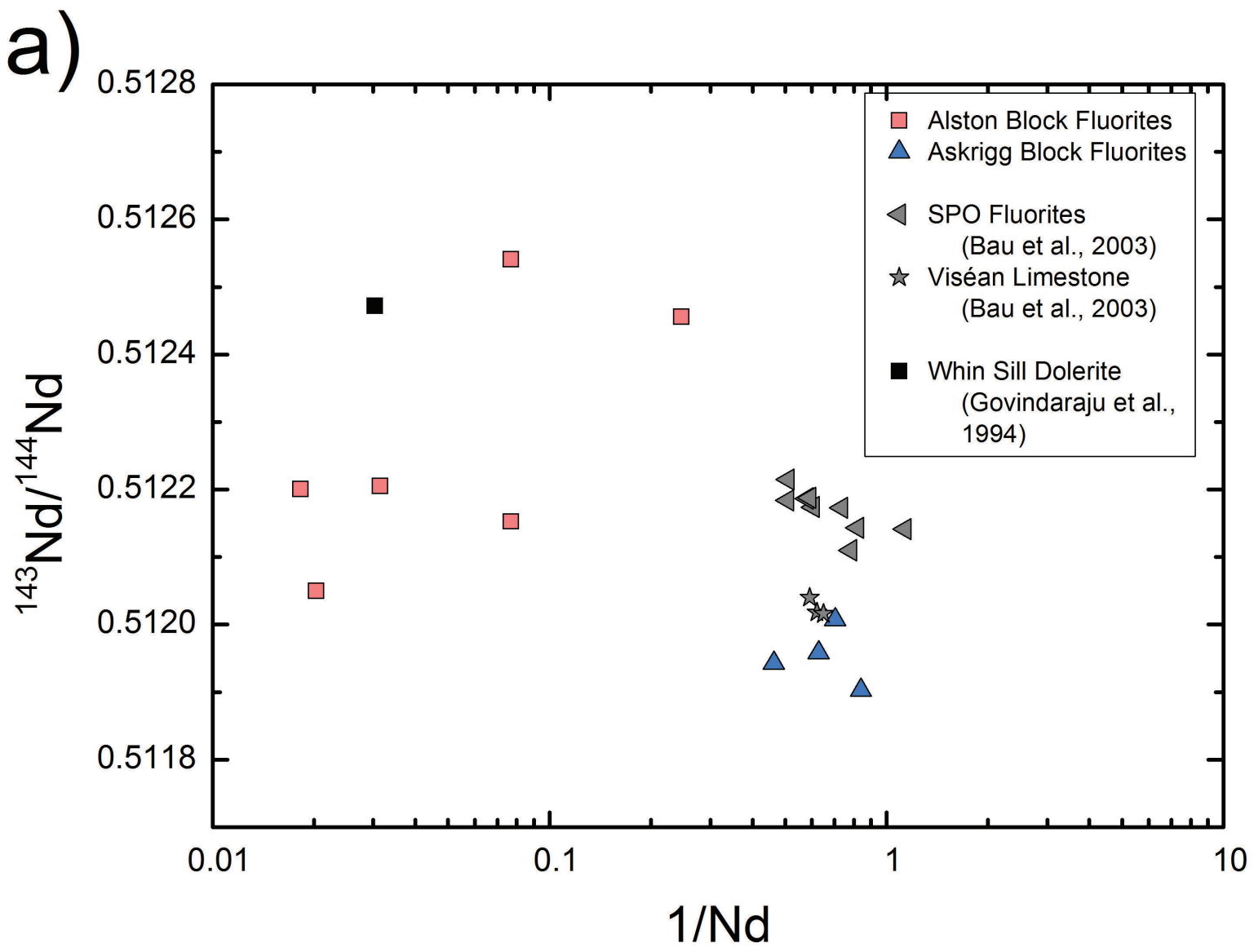
a)
0.5128
0.5126
0.5124
0.5122
0.5120
0.5118
$^{143}Nd/^{144}Nd$
0.01
0.1
1
10
1/Nd
Alston Block Fluorites
Askrigg Block Fluorites
SPO Fluorites
(Bau et al., 2003)
Viséan Limestone
(Bau et al., 2003)
Whin Sill Dolerite
(Govindaraju et al., 1994)

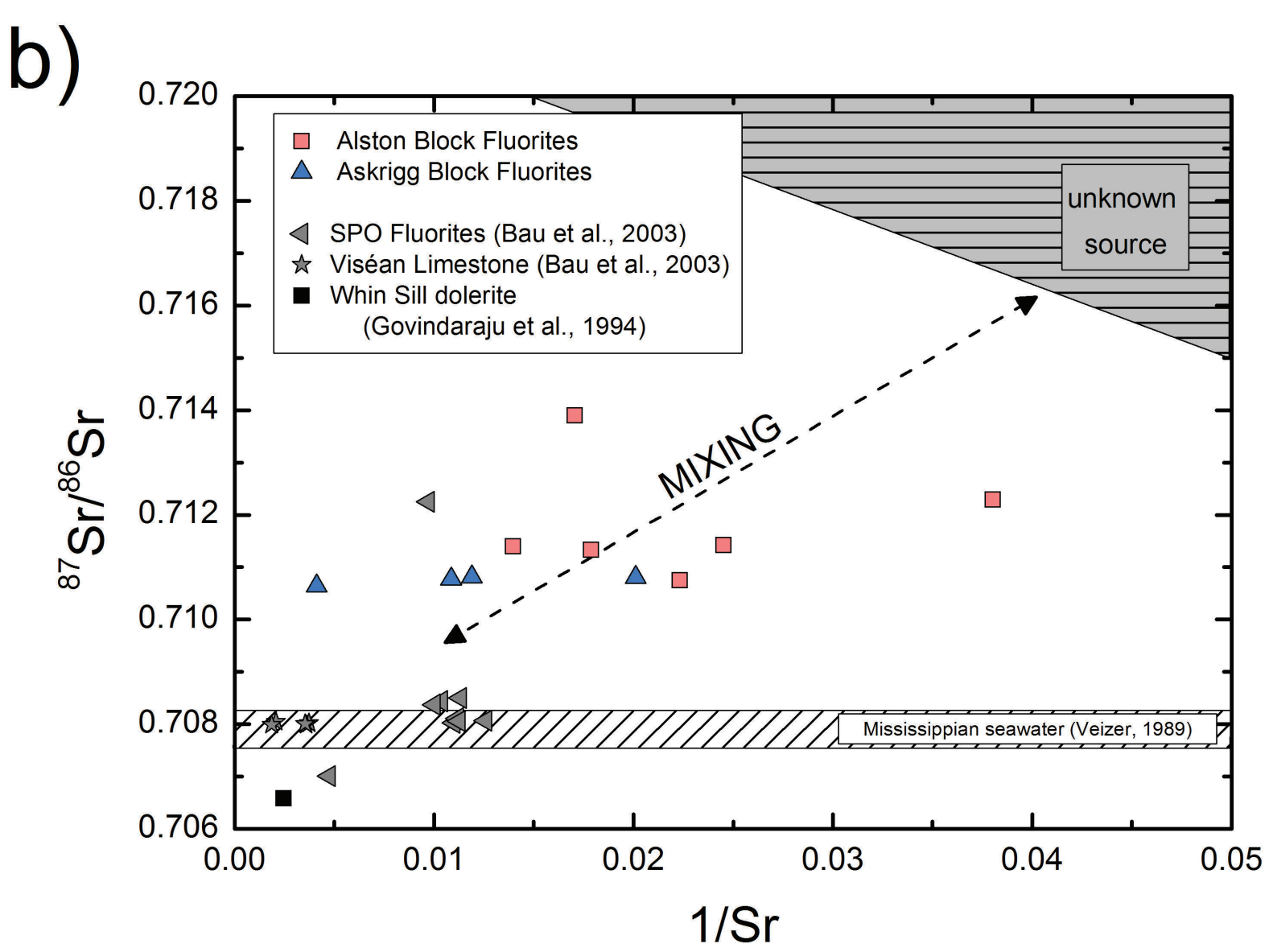
b)
Alston Block Fluorites
Askrigg Block Fluorites
SPO Fluorites (Bau et al., 2003)
Viséan Limestone (Bau et al., 2003)
Whin Sill dolerite
(Govindaraju et al., 1994)
unknown source
MIXING
Mississippian seawater (Veizer, 1989)
$^{87}Sr/^{86}Sr$
1/Sr
0.720
0.718
0.716
0.714
0.712
0.710
0.708
0.706
0.00
0.01
0.02
0.03
0.04
0.05

Table 1: Attributes of the two basement granites emplaced in the Northern Pennine Orefield.

Intrusion	**Weardale granite**	**Wensleydale granite**
	(Holland and Lambert 1970)	(Dunham 1974)
Emplaced in	Alston Block	Askrigg Block
Chemistry	calc-alkaline	calc-alkaline
	(Webb and Brown 1989)	(Webb & Brown, 1989)
Tectonic setting	subduction- and arc-collision	subduction- or within-plate
	(Webb & Brown, 1989)	(Webb & Brown, 1989)
Origin	Upper mantle (Webb & Brown, 1989)	Crust (Webb & Brown, 1989)
Age	420±10 Ma (Rb-Sr; Holland & Lambert, 1970)	410±10Ma (Rb-Sr; Dunham, 1974)
	398±1.6 Ma (Re-Os; Selby et al. 2008)	
	399.3 ±0.7Ma (U-Pb; Kimbell et al. 2010)	

Electronic supplementary material

Table 1: Samples from the Alston Block and corresponding results of crush-leach analysis.

			Crush-leach analyses (µg/kg) as analysed						
	Location	Grid Ref.	Na	K	Li	Cl	Br	Na/Br	Cl/Br
Fluorite									
AL96-1*	Coldberry	NY 940 292	9675	880	32	20136	41.66	232.2	483.3
AL96-2	Lodgesike	NY 953 293	17509	1590	32	52412	112.89	155.1	464.3
AL96-3	Flushiemere	NY 904 313	8475	1068	23	35204	77.67	109.1	453.3
AL96-4	Pike law	NY 901 316	2890	143	8	8971	25.02	115.5	358.6
AL96-5	West Rigg	NY 908 393	3150	201	12	11178	28.18	111.8	396.7
AL96-6	Whiteheaps	NY 949 466	34904	3101	54	50013	193.8	180.1	258.1
AL96-7	Middlehope	NY 895 406	33820	2950	80	56123	198.43	170.4	282.8
AL96-8	Burtree Pasture	NY 858 411	35596	3425	92	58355	221.06	161.0	264.0
AL96-9	Groverake	NY 895 442	12510	1006	29	65902	209.34	59.8	314.8
AL96-10/p*	Frazer's Hushes	NY 890 443	8040	587	18	22392	73.73	109.0	303.7
AL96-10/p	"	"	16153	1284	23	25385	76.22	211.9	333.0
AL96-10/g*	"	"	16372	1729	35	24720	77.74	210.6	318.0
AL96-11*	Scraithole	NY 808 456	30306	2703	78	53942	168.33	180.0	320.5
AL96-13	Langdon	NY 851 336	1210	64	2	4688	9.04	133.8	518.6
AL96-17	Dowgang	NY 778 418	3730	210	12	12361	32.47	114.9	380.7
Al96-19	Nenthead	NY 787 436	3120	186	14	14062	30.35	102.8	463.3
AL96-24/g	Cambokeels	NY 934 385	10290	1017	36	34191	37.37	275.4	914.9
AL96-24/p*	"	"	1580	78	33	4148	20.75	76.1	199.9
AL96-26*	Hilton	NY 763 225	10950	291	11	26422	124.38	88.0	212.4
AL96-27	Yewtree	NY 995 355	14620	887	32	35560	190.34	76.8	186.8
AL96-28/b	Heights	NY 926 389	10950	1304	52	27267	40.26	272.0	677.3
AL96-28/g	"	"	9992	1082	41	24134	39.86	250.7	605.5
Quartz									
AL96-2	Lodgesike	NY 953 293	1260	114	9	3739	20	63.0	187.0
AL96-5	West Rigg	NY 903 393	450	83	6	1026	7.39	60.9	138.8
AL96-6	Whiteheaps	NY 949 466	2370	102	7	5226	26.45	89.6	197.6
AL96-8	Burtree Pasture	NY 858 411	2010	86	5	5326	20.86	96.4	255.3
AL96-9	Groverake	NY 895 442	930	91	12	1924	12	77.5	160.3
AL96-12	Cowgreen	NY 810 311	4380	392	13	12299	94.37	46.4	130.3
AL96-17	Dowgang	NY 778 418	1870	77	13	4037	20.29	92.2	199.0
AL96-19	Nenthead	NY 787 436	2110	95	10	4670	27.8	75.9	168.0
GSV-1/c	Dorth Gill	NY 758 379	1950	509	10	5039	21.6	90.3	233.3
GSV-1/e	"	"	2320	519	14	5588	25.3	91.7	220.9
GSV-2/c	South Tyne river	NY 762 378	3150	338	16	7606	32.3	97.5	235.5
GSV-2/e	"	"	1940	264	14	4633	19.1	101.6	242.6
GSV	Noonstones Hill	NY 748 381	4200	379	17	9742	41.9	100.2	232.5
Calcite									
AL96-19	Nenthead	NY 787 436	9290	626	26	24903	146.78	63.3	169.7
Sphalerite									
AL96-19	Nenthead	NY 787 436	2756	176	10	7520	25.85	106.6	290.9
Barite									
AL96-12	Cowgreen	NY 810 311	4620	323	14	13921	83.17	55.5	167.4
AL96-13	Langdon	NY 851 336	807	350	26	1597	8.35	96.6	191.3
AL96-14	Bands	NY 830 322	5618	546	41	15737	72.59	77.4	216.8
AL96-15	Lady's Rake	NY 806 342	3224	365	21	10245	60.37	53.4	169.7
AL96-16	Grasshill	NY 815 352	5340	318	14	16520	114.06	46.8	144.8
AL96-19	Nenthead	NY 787 436	3847	374	48	16713	106.06	36.3	157.6
AL96-20	Closehouse	NY 840 227	2974	240	7	8162	41.56	71.6	196.4
AL96-21	Settlingstones	NY 842 642	48	12	7	1052	0.8	60.0	1315.0
AL96-22	Silverband	NY 705 319	1180	53	13	3545	17.09	69.0	207.4
AL96-23	East Cowgreen	NY 816 317	5221	292	7	15319	114.32	45.7	134.0

Samples in ***bold italics*** are those where REY were determined. Samples marked with an asterisk are those were Sr and Nd isotopes were determined.

Table 2: Samples from the Askrigg Block and corresponding results of crush-leach analysis.

			Crush-leach analyses (µg/kg) as analysed							
	Location	Grid Ref.	Na	K	Li	Cl	Br	SO_4	Na/Br	Cl/Br
Fluorite										
AS96-1	Trollers' Gill	SE 068 618	900	35	2	1864	7.9	25	113.9	235.9
AS96-2	Grassington	SE 027 668	940	39	4	1965	9.5	164	98.9	206.8
AS96-4	NW Kettlewell	SD 952 727	5200	177	11	11017	49.8	401	104.4	221.2
AS96-5/p	NE Kettlewell	SD 974 736	1670	50	2	2685	10.9	60	153.2	246.3
AS96-5*	"	"	2510	153	3	4983	25.3	180	99.2	197.0
AS96-6*	Haw Bank	SD 986 898	11000	528	12	20934	110.4	527	99.6	189.6
AS96-7	Coldstone Quarry	SE 109 640	2120	75	2	4057	16.8	89	126.2	241.5
AS96-13*	Langthwaite	SD 997 026	5280	216	6	10830	43.2	40	122.2	250.7
AS96-14*	Hungry Hushes	NY 985 028	2230	77	3	5326	18.7	64	119.3	284.8
AS96-15	Surrender Ground	NY 975 025	9460	298	8	18688	93.2	86	101.5	200.5
AS96-16	Forefield Rake	NY 967 025	4710	158	5	10690	37.1	48	127.0	288.1
AS96-17	Hebden Gill	SD 025 656	12320	442	13	22121	111.8	202	110.2	197.9
Quartz										
AS96-4	NW Kettlewell	SD 952 727	11850	405	9	23268	116.1	189	102.1	200.4
AS96-5	NE Kettlewell	SD 974 736	4320	151	4	8325	45.2	63	95.6	184.2
AS96-6	Haw Bank	SD 986 898	3900	566	9	10208	47.7	706	81.8	214.0
AS96-7	Coldstone Quarry	SE 109 640	11790	432	9	21951	111.5	48	105.7	196.9
AS96-9	Marrick Moor	NZ 063 004	1061	323	4.2	2365	16.5		64.3	143.3
AS96-14	Hungry Hushes	NY 985 028	950	41	4	2775	16	271	59.4	173.4
AS96-16	Forefield Rake	NY 967 025	16550	650	14	36475	186.8	212	88.6	195.3
Calcite										
AS96-8	Cobscar Rake	SE 060 930	206	125	4.4	170	0.83		248.2	204.8
AS96-9	Marrick Moor	NZ 063 004	200	118	3.8	163	0.73		274.0	223.3
AS96-10	Hurst	NZ 050 024	5280	217	10	11432	30.8		171.4	371.2
AS96-11	Stang Mine	NZ 008 057	6270	279	13	17293	113.2		55.4	152.8
AS96-12	Windegg Lead level	NZ 013 052	266	107	14	300	1.47		181.0	204.1
AS96-13	Langthwaite	NY 997 026	150	52	10	136	0.61		245.9	223.0
AS96-16	Forefield Rake	NY 967 025	94	287	5.5	125	0.61		154.1	204.9
Sphalerite										
AS96-6	Haw Bank	SD 986 898	6760	1401	10	23880	83.1		81.3	287.4
AS96-17	Hebden Gill	SE 025 656	1680	89	3	3944	11.2		150.0	352.1
Barite										
AS96-3	Grassington	SE 021 657	440	68	4	1566	3.2		137.5	489.4
AS96-7	Coldstone Quarry	SE 109 640	390	33	3	772	4		97.5	193.0
AS96-8	Cobscar Rake	SE 060 930	507	130	33	832	2.9		174.8	286.9
AS96-9	Marrick Moor	NZ 063 004	516	357	212	838	4.4		117.3	190.5
AS96-10	Hurst	NZ 050 024	47	70	71	119	0.65		72.3	183.1
AS96-14	Hungry Hushes	NY 985 028	1163	50	15	2035	5.9		197.1	344.9
AS96-15	Surrender Ground	NY 975 025	1675	63	91	3357	16.6		100.9	202.2
AS96-16	Forefield Rake	NY 967 025	5500	333	15	13078	62		88.7	210.9
AS96-17	Hebden Gill	SE 025 656	1050	64	9	2452	12.2		86.1	201.0
AS96-18	Yarnbury	SE 020 654	3740	383	13	11769	88.3		42.4	133.3

Samples in ***bold italics*** are those where REY were determined. Samples marked with an asterisk are those were Sr and Nd isotopes were determined.

Table 3: Microthermometry data retrieved from fluid inclusion assemblages in Alston and Askrigg Block mineralization.

Region	Mineral	T_e	T_{hyd}	T_{ice}	T_h	Salinity [wt% NaCl equiv]
Alston Block	Fluorite	-52 to -80°C	-23 to -26°C	-15.5 to -21°C	105 to 159°C	19.7-22.7
	Quartz	-50 to -70°C		-17.5 to -22.7°C	105 to 158°C	20.5-23
	Barite	-56 to -60°C		-14.5 to -17°C	110 to 160°C	18.4-20.4
	Calcite	-50°C		-17.8 to -19.7°C	104-134°C	21.2-22.5
Askrigg Block	Fluorite	-36 to -59°c	-21.7 to -31°C	-18.1 to -26°C	99-160°C	19-26
	Barite	-42 to -74°C	-19 to -24°C	-9.7 to -19°C	110-173°C	12.4-21.6

Table 4: Barium, rare earth element and Y concentrations in fluorite specimen from the Alston Block.

mg kg^{-1}	AL96-1	AL96-2	AL96-3	AL96-4	AL96-5	AL96-6	AL96-7	AL96-8	AL96-10/p	AL96-10/g	AL96-11	AL96-13	AL96-17	AL96-19	AL96-24/p	AL96-26
Ba	6.83	14.9	2.09	5.64	31.9	1.52	0.987	4.57	13.8	2.31	5.98	7.99	6.51	7.55	1.13	1850
La	6.19	6.39	4.49	4.48	8.76	32.4	9.81	25.5	28.4	56.6	14	15.9	37.9	20	4.43	1.15
Ce	13.8	19	10.8	15.6	18.3	68.5	19.2	47.3	59.3	102	34.6	32.3	75.3	44.8	12.4	3.62
Pr	2.35	3.17	1.76	3.31	2.79	9.4	2.83	6.28	9.34	12.2	5.85	5.2	10.3	7.11	2.28	0.637
Nd	13	19.3	9.23	21.8	16.1	43.7	14.7	29.1	49.3	54.8	31.8	28.3	49.6	36.3	13	4.06
Sm	7.76	11	5.78	14.8	12.9	21.8	10.9	12	25.9	27.6	17	14.9	22.6	20.4	7.97	2.88
Eu	14.9	23.2	5.41	38.9	21.9	22.2	19.2	27.6	62.8	65.6	47.2	41.8	52.3	54.6	2.89	0.868
Gd	18.8	25.6	13.4	35.5	35.6	44.5	29.8	24.9	56	50.6	40.4	32.3	44.5	47.5	15.8	7.2
Tb	3.15	4.12	2.38	6.13	7.01	9.2	5.83	4.53	8.05	7.97	6.64	5.2	7.44	7.43	2.95	1.37
Dy	18.2	22.2	11.9	33.8	42.3	47.6	32.2	23.8	43.7	47.2	31	28.9	38.2	39.2	17.1	8.97
Y	252	294	152	363	381	551	311	200	552	382	372	351	356	436	222	135
Ho	2.79	3.35	1.56	5.05	6.62	7.07	4.88	3.37	6.72	6.61	4.68	4.14	5.49	6.18	2.57	1.48
Er	5.96	7.11	3.28	10.4	14.9	17.1	11	7.92	14.6	14.1	10.4	8.75	12.1	13.2	6.21	3.39
Tm	0.549	0.663	0.296	0.997	1.46	1.94	1.11	0.838	1.27	1.29	0.96	0.861	1.16	1.18	0.714	0.334
Yb	2.48	3.02	1.24	4.4	7.46	10.5	5.54	4.21	5.6	7.14	3.96	4.02	5.67	5.47	4.26	1.83
Lu	0.239	0.29	0.107	0.417	0.748	1.12	0.592	0.422	0.598	0.772	0.416	0.397	0.587	0.582	0.433	0.168
∑REY	362.2	442.4	223.6	558.6	577.9	888.0	478.6	417.8	923.6	836.5	620.9	574	719.1	740	315.0	173
Y/Ho	90.3	87.8	97.4	71.9	57.6	77.9	63.7	59.3	82.1	57.8	79.5	84.8	64.8	70.6	86.4	91.2
Ce_{SN}/Ce^{*}_{SN}	1.36	1.96	1.24	2.43	1.74	1.16	1.34	1.19	1.30	1.26	1.31	1.38	1.24	1.20	1.39	2.35
Eu_{SN}/Eu^{*}_{SN}	5.55	6.40	2.68	7.51	4.07	2.88	4.27	6.95	8.17	8.33	8.22	8.87	7.56	8.25	1.11	0.79

Table 5: Barium, rare earth element and Y concentrations in fluorite specimen from the Askrigg Block.

mg kg^{-1}	AS96-1	AS96-5/p	AS96-6	AS96-7	AS96-7 Rep	AS96-13	AS96-14	AS96-17
Ba	3.38	37600	<d.l.	71.7	66.5	<d.l.	392	72200
La	0.227	0.642	0.508	0.306	0.318	0.514	0.25	0.864
Ce	0.469	1.19	1.63	0.684	0.751	1.55	0.855	2.02
Pr	0.1	0.23	0.379	0.143	0.152	0.298	0.222	0.428
Nd	0.519	1.19	2.16	0.83	0.823	1.59	1.42	2.36
Sm	0.223	0.448	0.845	0.358	0.35	0.683	0.748	1.02
Eu	0.0939	BaO	0.282	0.133	0.144	0.249	0.291	BaO
Gd	0.579	0.837	1.82	0.86	0.951	1.33	1.8	2.24
Tb	0.078	0.112	0.326	0.131	0.129	0.225	0.348	0.365
Dy	0.555	0.721	2.21	0.986	0.944	1.73	2.29	2.42
Y	18.2	18.9	41.4	31	28.9	37.5	43.2	54.3
Ho	0.118	0.142	0.427	0.21	0.222	0.352	0.434	0.488
Er	0.285	0.331	1.13	0.5	0.554	0.892	1.13	1.32
Tm	0.0218	0.0256	0.13	0.0444	0.0472	0.0849	0.123	0.131
Yb	0.094	0.119	0.632	0.192	0.199	0.474	0.63	0.635
Lu	0.0103	0.0135	0.0701	0.0207	0.0232	0.0592	0.0706	0.0801
∑REY	21.6	24.9	54.0	36.4	34.5	47.5	53.8	68.7
Y/Ho	154.2	133.1	97.0	147.6	130.2	106.5	99.5	111.3
Ce_{SN}/Ce^{*}_{SN}	0.93	1.01	1.10	1.29	1.08	1.10	1.63	1.09
Eu_{SN}/Eu^{*}_{SN}	1.33		0.99	1.14	1.26	1.19	1.03	

Table 6: Sr and Nd isotopes in fluorite specimen from the NPO. JDo-1 and IF-G were used as CRM. Reference value for $^{87}Sr/^{86}Sr$ obtained from Ohno & Hirata (2007) and $^{143}Nd/^{144}Nd$ obtained from Alexander et al. (2009).

SAMPLE	[Nd] mg kg^{-1}	[Sr] mg kg^{-1}	$^{143}Nd/^{144}Nd$	+/-2σ	$^{87}Sr/^{86}Sr$	+/-2σ
AL96-1	13.0	40.8	0.512153	5	0.711420	4
AL96-10/p	49.3	58.6	0.512050	4	0.713896	4
AL96-10/g	54.8	55.9	0.512201	3	0.711330	5
AL96-11	31.8	71.6	0.512206	5	0.711399	4
AL96-24	13.0	26.3	0.512541	5	0.712295	4
AL96-26	4.06	44.8	0.512456	4	0.710751	4
AS96-5	1.19	243	0.511903	22	0.710639	4
AS96-6	2.16	92.1	0.511943	21	0.710772	3
AS96-13	1.59	84.0	0.511959	8	0.710813	4
AS96-14	1.42	49.7	0.512007	29	0.710807	7
JDo-1	-	-	0.512248	5	0.707548 (Ref: 0.70752)	5
IF-G	-	-	0.511379 (Ref: 0.511258)	6	0.719517	6